Colour figures and captions appended at the end

Paleoclimate Variability in the Mediterranean and Red Sea Regions during the Last 500,000 Years

Implications for Hominin Migrations

by Eelco J. Rohling, Katharine M. Grant, Andrew P. Roberts, and Juan-Cruz Larrasoaña

The Mediterranean–Red Sea region has been critical to dispersal of hominids and other species between Africa and the rest of the world, and climate and sea level are thought to be key controls on migration pathways. Assessing climate variations, we highlight increased millennial-scale variability at 480–460, 440–400, 380–360, 340–320, 260–220, 200–160, 140–120, and 80–40 thousand years ago (ka), which likely caused intermittent habitat fragmentation. We also find that passageways across the Sahara Desert and the northern out-of-Africa route (from Egypt into the Levant) were intermittently open during pluvials associated with orbital insolation maxima. No such relationship is apparent for the southern out-of-Africa route (across the Red Sea). Instead, we present a novel interpretation of combined sea-level and regional climate control on potential migrations via the southern route, with "windows of opportunity" at 458–448, 345–340, 272–265, 145–140, and 70–65 ka. The 145–140 ka window seems relevant for early colonization of Arabia at 127 ± 16 ka, and the 70–65 ka window agrees with estimates of 65 +5/−8 ka for the final out-of-Africa migration by the anatomically modern human founder group of all non-Africans. Once they reached Eurasian Mediterranean margins, populations benefited from a rich diversity of terrain and microclimates, with persistent favorable conditions in lowlands and potential to occupy higher elevations during milder periods.

Introduction

The Mediterranean–Red Sea region occupies a zone that is influenced by four major climate systems. From northwest to southeast, these are (1) the temperate westerlies that affect Europe, the western Mediterranean, and the northern sector of the eastern Mediterranean; (2) the dry subtropical conditions that dominate the southern and eastern sectors of the Mediterranean basin as well as the entire Red Sea region; (3) the African monsoon, which affects Mediterranean conditions through inflow of major rivers (Nile, and in the past other North African drainage systems) and that has caused past contractions and expansions of the Sahara desert; and (4) the Indian Ocean monsoon, which causes seasonal wind reversals over the southern Red Sea region up to latitudes of 20°–25°N. No significant rainfall is associated with the Indian Ocean monsoon over the Red Sea and Arabian Peninsula today, but the monsoon's summer rainfall domain may have shifted onto the southeast margin of the Arabian Peninsula (i.e., Yemen and Oman) during insolation-driven monsoon maxima such as those of the Early-Middle Holocene (Conroy and Overpeck 2011).

Climatic gradients over the Mediterranean and Red Sea region are well illustrated by the updated Köppen-Geiger climate classification (Kottek et al. 2006; fig. 1). Important measures of climate variability through time are obtained from a variety of methods, such as pollen data, lake levels, stable isotopes from a variety of sedimentary archives, faunal changes, and others. These data especially supply information about changes in regional temperature and precipitation regimes. In addition, the Red Sea has in the past decade become a key region for reconstruction of continuous records of sea-level fluctuations (Grant et al. 2012; Rohling et al. 1998*a*, 2008*a*, 2008*b*, 2009*b*, 2010; Siddall et al. 2003, 2004). Finally, the presence of vast deserts to the south of the Mediterranean

Eelco J. Rohling is Professor, **Katharine M. Grant** is Postdoctoral Researcher, and **Andrew P. Roberts** is Professor at the Research School of Earth Sciences of the Australian National University (Canberra, Australian Capital Territory 0200, Australia [eelco.rohling@anu.edu.au; katharine.grant@anu.edu.au; andrew.roberts@anu.edu.au]). **Juan-Cruz Larrasoaña** is Staff Scientist at the Instituto Geológico y Minero de España of Unidad de Zaragoza (Zaragoza 50006, Spain [jc.larra@igme.es]). This paper was submitted 3 VII 13, accepted 4 IX 13, and electronically published 18 XII 13.

 0011-3204/2013/54S8-00XX$10.00. DOI: 10.1086/673882

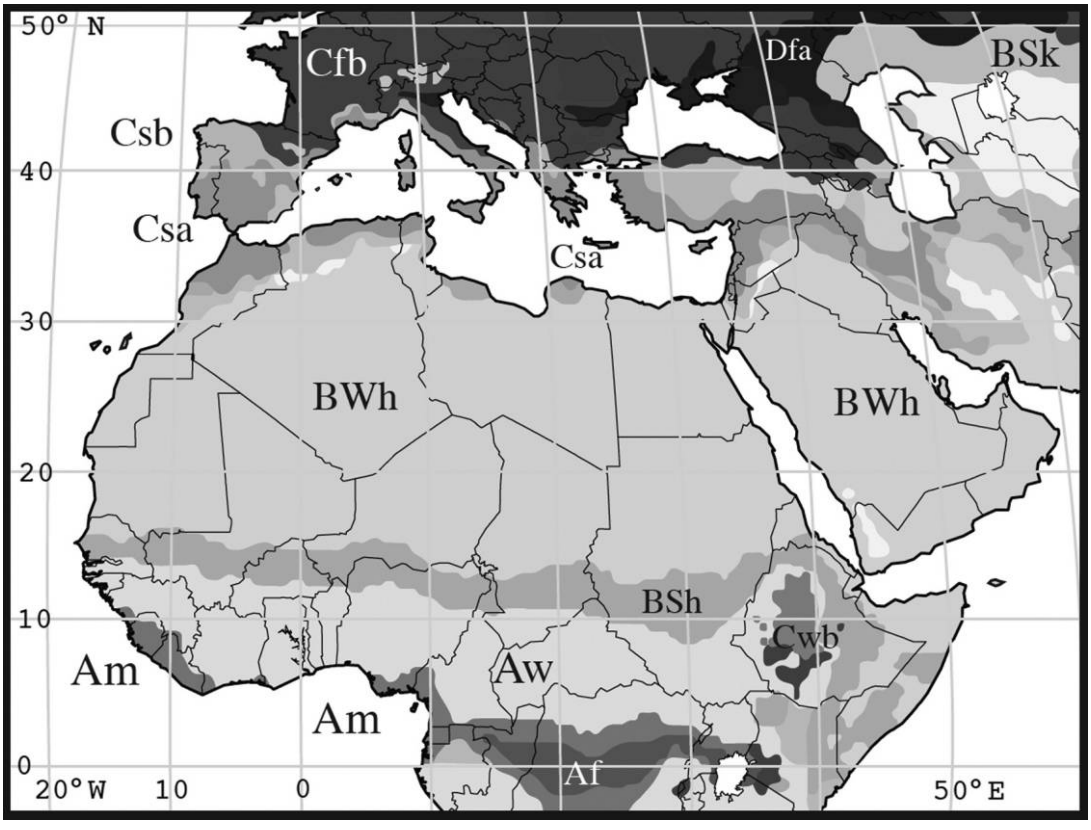

Figure 1. Summary map of the main climate zones in the study region using the Köppen-Geiger climate classification. A = equatorial; B = arid; C = warm temperate; D = snow; s = summer dry; f = fully humid; S = steppe; W = desert; w = winter dry; m = monsoonal; a = hot summer; b = warm summer; k = cold arid; h = hot arid. Modified after Kottek et al. (2006). A color version of this figure is available in the online edition of *Current Anthropology*.

and around the Red Sea gives rise to large windblown dust fluxes into these basins, and reconstructions of those fluxes through time—notably using marine sediment cores—also reveal important changes in regional climate conditions.

In this paper, we present an overview of the modern climate of the region and of the main changes that have been reconstructed from paleoclimate proxy records for the last 500,000 yr. This overview provides a context for consideration of the role of climate variability in anthropological and archaeological developments at the interface of Africa and Europe.

Modern Climatic Setting

Mediterranean

We summarize modern Mediterranean climate conditions following the recent review of Rohling et al. (2009*a*). The classical Mediterranean climate is characterized by warm and dry summers and mild and wet winters. Mean annual precipitation along the Mediterranean ranges from less than 0.12 m in North Africa, to over 2.00 m in portions of southwest Turkey and in the eastern Adriatic Sea along the slopes of the Dinaric Alps (Naval Oceanography Command 1987). Total evaporation in the entire Mediterranean increases toward the east, with an average of 1.45 m y^{-1} (Malanotte-Rizzoli and Bergamasco 1991) to 1.57 m y^{-1} (Béthoux and Gentili 1994).

The classical Mediterranean climate is a result of the region's location on the transition between temperate westerlies that dominate over central and northern Europe and the subtropical high-pressure belt over North Africa (fig. 2; Boucher 1975; Lolis, Bartzokas, and Katsoulis 2002). In summer, subtropical high-pressure conditions (and drought) extend from the southeast in a northwestward direction over most of the Mediterranean. Polar-front depressions may still reach the western Mediterranean, but they only exceptionally penetrate the eastern Mediterranean (Rohling and Hilgen 1991). During winter, the subtropical conditions shift southward, and the northern sector of the Mediterranean becomes influenced by the temperate westerlies with associated Atlantic depressions that track eastward over Europe. These depression influences extend from the Mediterranean southeastward across the Levant and into the northernmost sector of the Red Sea (e.g., Arz et al. 2003*a*; Bar-Matthews et al. 2003; Goodfriend 1991; Matthews, Ayalon, and Bar-Matthews 2000; McGarry et al. 2004; Trommer et al. 2010).

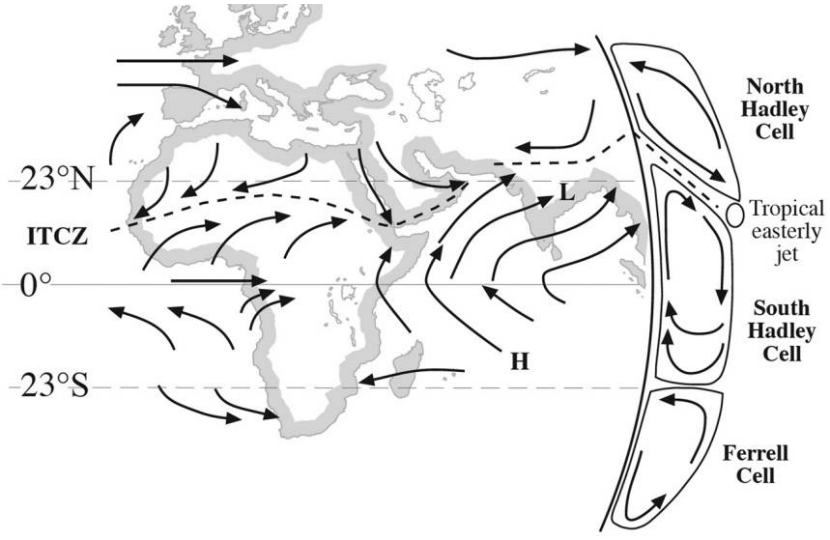

Figure 2. Atmospheric circulation pattern during Northern Hemisphere summer. The main winds are indicated by arrows. ITCZ = intertropical convergence zone; H = areas of high sea-level pressure; L = areas of low sea-level pressure. After an adaptation in Rohling et al. (2009), which compiled information from Rossignol-Strick (1985) and Reichart (1997).

Polar and continental air masses over Europe are channeled into the Mediterranean basin through gaps in the mountainous topography of the northern Mediterranean margin. During winter and spring, intense cold and dry air flows through the lower Rhone Valley to reach the Gulf of Lions (the "mistral"), and similar flows extend over the Adriatic and Aegean Seas (the "Bora" and "Vardar"), where they cause strong evaporation and sea surface cooling (e.g., Casford et al. 2003; Leaman and Schott 1991; Maheras et al. 1999; Poulos, Drakopoulos, and Collins 1997; Saaroni et al. 1996; and references therein). The northerly air flows into the western and eastern Mediterranean are determined by interaction between an intense low over the central or eastern Mediterranean and northeastward extension of the Azores High (over Iberia, France, and southern Britain) or westward ridging of the Siberian High toward northwestern Europe and southern Scandinavia (Lolis, Bartzokas, and Katsoulis 2002; Maheras et al. 1999). Persistent winter low-pressure conditions over the region result from high Mediterranean sea surface temperatures (Lolis, Bartzokas, and Katsoulis 2002).

The most pronounced basin-wide cold winter events complement cold conditions over Europe and develop in association with positive sea-level pressure anomalies to the west or northwest of the British Isles and particularly low pressure over the Mediterranean. An important aspect of winter variability concerns cyclogenesis (formation of new depressions), which governs precipitation in the northeastern and south-central sectors of the Mediterranean. Some Atlantic depressions may enter the (western) basin, but most cyclones observed in the Mediterranean form over the basin itself (Rumney 1968; Trigo, Davies, and Bigg 1999), when cold and relatively dry northerly air flows extend over warm sea surfaces in the northern sectors of the basin. Thus, winter cyclones are linked to North Atlantic systems, given that they represent either (occasional) direct entries of Atlantic synoptic systems into the Mediterranean basin or secondary lows formed when Atlantic systems interact with the Alps and lead to cyclogenesis within the basin (Trigo, Davies, and Bigg 2000).

Over the Mediterranean Sea, cyclogenesis is most frequent over the Gulf of Genoa and the Ligurian Sea, but the Aegean Sea is also a major center for winter cyclogenesis (Boucher 1975; Cantu 1977; Rumney 1968; Trewartha 1966; Trigo, Davies, and Bigg 1999). Most Genoan depressions track over Italy, thereby affecting the Adriatic region, and thence in a generally eastward direction toward the Aegean Sea and/or northern Levantine seas (Lolis, Bartzokas, and Katsoulis 2002; Rumney 1968; Trewartha 1966; Trigo, Davies, and Bigg 1999). These depressions, along with those that develop over other centers of cyclogenesis, cause the winter precipitation that is characteristic of modern Mediterranean climate. Geological archives indicate that Mediterranean depressions have controlled Mediterranean climate in the Levant as an enduring feature over glacial-interglacial timescales (Bar-Matthews et al. 2003; Goodfriend 1991; Matthews, Ayalon, and Bar-Matthews 2000; McGarry et al. 2004; Rohling 2013; and references therein).

Summer rainfall is low around the Mediterranean region, especially in eastern and southeastern sectors. Some cyclogenesis occurs around Cyprus and the Middle East in summer, but adiabatic descent in the upper troposphere—related to the Asian summer monsoon—precludes deep convection over the region and so causes the prevalence of dry summer con-

ditions (Rodwell and Hoskins 1996; Trigo, Davies, and Bigg 1999).

The African monsoon does not reach directly into the Mediterranean basin, and there is no evidence that it ever did during the Quaternary. It does, however, have (or more appropriately used to have) a "remote" influence on the basin through Nile River discharge. Before the anthropogenic control of the Nile, its average discharge was 8.4×10^{10} m^3 yr^{-1} (4.5×10^{10} m^3 yr^{-1} in low-flood years to 15.0×10^{10} m^3 yr^{-1} in high-flood years), which from the mid-1960s has dwindled to nearly nothing (Béthoux 1984; Nof 1979; Rohling and Bryden 1992; Said 1981; Wahby and Bishara 1981). During the predamming instrumental era, a strong (threefold) interannual variability has been noted between high and low discharge years, mainly due to variability in the monsoon-fed contribution of the Blue Nile and Atbara rivers (see data summary in Rohling et al. 2009*a*).

The Nile River comprises two different systems: the White Nile, which drains the equatorial uplands of Uganda in a regular, permanent manner; and the Blue Nile and Atbara, which drain highly seasonal (summer) African monsoon precipitation from the Ethiopian highlands. Summarizing the predamming Nile hydrology after Adamson et al. (1980) and Williams et al. (2000), it appears that up to 30% of the annual discharge of the Nile originated from the White Nile and a minimum of 70% of the annual discharge from the Blue Nile/Atbara. The winter flow was dominated (83%) by the steady White Nile contribution, and the Blue Nile/Atbara component provided 90% of the summer flow (with a peak over August–October). The White Nile discharge has a much smaller ratio of change between its annual peak and lowest monthly value, with a maximum between late September and January.

It should be noted that the Nile has not always been the only route for drainage of African monsoon precipitation into the Mediterranean. During past monsoon maxima (related to orbitally induced insolation maxima), the extent of the Sahara desert was much reduced, and there was northward routing of drainage from the central Saharan watershed into the Mediterranean along the wider North African margin (see below for details).

Red Sea

The Red Sea basin is entirely situated in an arid zone with very low humidity. Coastal stations record annual rainfall figures of less than 20 mm in the north and 50–100 mm in the south (Pedgley 1974). Riverine flow into the basin is negligible because of the basin's small watershed (Maillard and Soliman 1986; Morcos 1970; Siddall et al. 2004; fig. 3). One of the larger systems that drains into the Red Sea is the Baraka (Tokar) wadi in Sudan, which today is active 40–70 d yr^{-1} (mainly during autumn). Wadi Baraka discharges 200–970×10^6 m^3 water at 18.5°N into the Red Sea (Trommer et al. 2011; Whiteman 1971), which is equivalent to a maximum of only 2 mm y^{-1} when distributed over the entire Red Sea surface area. Thus, river inflow and precipitation are negligible throughout the Red Sea region, especially when contrasted with the high rates of evaporation, which seasonally reach 2 m y^{-1} or more (Maillard and Soliman 1986; Morcos 1970; Pedgley 1974; Privett 1959; see also Fenton et al. 2000; Siddall et al. 2004). Evaporation over the Red Sea is seasonally affected by atmospheric circulation changes that are related to the Indian Ocean monsoon. The most notable feature is a seasonal wind reversal over the southern Red Sea, the general nature of which is discussed below. For more details and modeling, see Jiang et al. (2009).

During winter (October–May), reduction of sensible heat radiation occurs over the cold landmass of central Asia that is enhanced by snow-induced high albedo (reflection of insolation) over the Tibetan Plateau and Himalayas. This results in a quasi-stable high-pressure system that extends from Mongolia to central Europe, Turkey, and Arabia. The cold, descending air leads to a radial outflow of cold dry air toward low-pressure areas over the relatively warm Indian Ocean. The intertropical convergence zone (ITCZ) is displaced southward in winter, to 20°S over East Africa, and the winter northeast monsoon blows across the Arabian Sea and the Gulf of Aden toward central Africa (Morcos 1970). A general southeasterly wind circulation results between a continental depression over central Africa and a continental anticyclone that extends from Asia to Arabia. Channeling by the rift geometry of the Red Sea coast then causes strong (6.7–9.3 m s^{-1}) winds to blow from the south or south-southeast over the southern half of the Red Sea up to about 20°N (e.g., Morcos 1970; Patzert 1974). Throughout October–December, there is a convergence between these south-southeasterlies and the north-northwesterly winds that prevail year-round over the northern Red Sea. This convergence occupies a north-south zone across the Red Sea at around 20°N (Jiang et al. 2009; Pedgley 1974), which varies in size and is characterized by low-pressure calms (Morcos 1970). Jiang et al. (2009) demonstrated that the position of the convergence zone may be determined by gaps in the topography, notably the Tokar Gap some 50 km inland from the Tokar Delta on the Sudan coast, which acts as an outlet of surface wind from the Red Sea basin in winter (and as an inlet in summer; see below).

During summer (June–September), the monsoon system is reversed. The spring melt reduces albedo over central Asia, and insolation increases, thereby causing the landmass to warm. This warms the air above, causing it to rise, creating a quasi-stable low-pressure system over northern India (<995 mb; Morcos 1970), which extends over Pakistan to the Persian Gulf. The updraft causes humid, relatively cool, maritime air to flow in from the area of higher pressure over the now relatively cool Indian Ocean. Latent heat release from condensation/precipitation against the flanks of the Himalayas fuels further deepening of the continental low-pressure cell and consequently more inflow of maritime air, which reinforces the system. The ITCZ reaches its most northerly po-

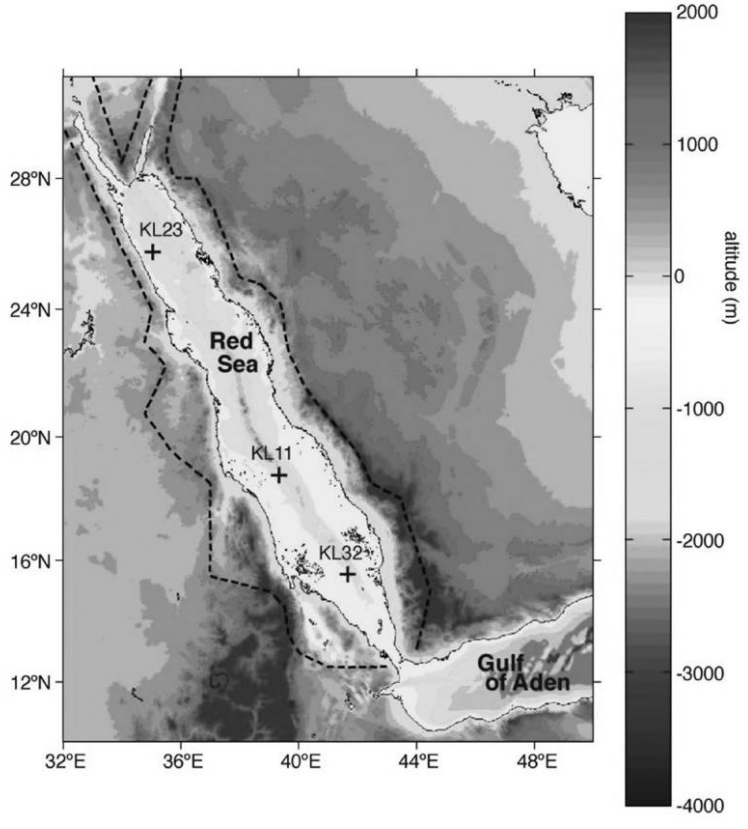

Figure 3. Topography of the Red Sea basin. The dashed line delineates the Red Sea watershed. Numbers refer to key sediment core locations (not used here). After Siddall et al. (2004). A color version of this figure is available in the online edition of *Current Anthropology*.

sition (20°N) in July and becomes identified with the front of the southwest monsoon. This passes north of Aden, and the southwest monsoon flows in a clockwise direction over East Africa, the Gulf of Aden, and the Arabian Sea toward the main monsoon low of northern India (Morcos 1970). At this time, a general northwesterly circulation is set up on the western side of the summer Asiatic low-pressure cell. This causes relatively weak (2.4–4.4 m s^{-1}) north-northwesterly or northwesterly winds to dominate over the entire length of the Red Sea (e.g., Morcos 1970; Patzert 1974).

Jiang et al. (2009) analyzed regional patterns superimposed on the general along-axis wind systems, which are more zonal (west to east or east to west) in nature and that are related to gaps in the topography along the basin, such as the Tokar Gap. There are eastward-blowing wind jets in summer (mainly through the Tokar Gap) and westward-blowing wind jets in winter from the Saudi Arabian margin (mainly over the northern Red Sea). Wind speeds in these surface jets can reach 10–15 m s^{-1}, and Jiang et al. (2009) provide clear evidence of atmospheric dust entrainment over the Red Sea. Jiang et al. (2009:5) further note that "other strong zonal winds . . . blow from the Egyptian coast eastward across the Red Sea longitudinal axis. . . . This . . . can also drive dust storms."

In the northernmost Red Sea, records of past climate change have detected an influence of southeast Mediterranean climate influences that extend across the Middle East (Arz et al. 2003*a*; Legge, Mutterlose, and Arz 2006; Trommer et al. 2010). Contemporary climatology suggests that this link functions through winter frontal rainfall associated with Cyprus lows (El-Fandy 1946; Morcos 1970).

Past Climate Variability

Glacial-Interglacial Changes

Throughout the last three million years, climate variability over the entire study region has been dominated by the effects of global ice-age cycles, which were particularly prominent during the last 500,000 yr (e.g., Lisiecki and Raymo 2005), with variability that is forced by cyclic changes in the earth-sun orbital configuration. The astronomical forcing of climate takes place because of three main processes, namely: changes in the eccentricity of the earth's orbit around the sun, with

climate effects in approximately 100- and 400-kyr cycles; changes in the tilt of the earth's rotational axis, with effects on climate in 41-kyr cycles; and precession of the equinoxes, with climate effects in cycles of 19- and 23-kyr durations (e.g., Berger 1977; Hays, Imbrie, and Shackleton 1976; Imbrie and Imbrie 1980, 1986; Milankovitch 1941).

Glaciations were strongly focused on the North American and northern Eurasian locations of continental ice sheets, but the effects on climate were global. This had global implications for sea level, with fluctuations between interglacial highstands up to +10 m (Kopp et al. 2009; Muhs et al. 2011; Rohling et al. 2008*b*, 2009*b*) and glacial lowstands at −120 m or lower relative to present sea level (Rohling et al. 1998*a*; Waelbroeck et al. 2002). Methods for constructing continuous records of sea-level variability now exist for the last half-million years (Rohling et al. 2009*b*, 2010; Siddall et al. 2003; Waelbroeck et al. 2002). Model-based deconvolutions of deep-sea stable oxygen isotope records have also been used to extend the record over many millions of years (Bintanja, van de Wal, and Oerlemans 2005; De Boer et al. 2010, 2011), but these still require independent validation (fig. 4).

Along with enlarged land-ice volumes, another defining characteristic of glacials was widespread cooling (e.g., CLIMAP Project Members 1976; MARGO Project Members 2009; Rohling et al. 2012; Schneider von Deimling et al. 2006). In the study region, cooling produced a strong gradient from west to east through the Mediterranean and then to the southeast along the axis of the Red Sea. Relative to the present, glacial sea surface temperatures in summer were reduced by 8° ± 2°C in the westernmost Mediterranean, 5° ± 2°C around Sicily, and 3° ± 2°C in the easternmost Mediterranean; winter sea surface temperatures were reduced by 5° ± 2°C, 3° ± 1°C, and 0°–2.5°C, respectively (Hayes et al. 2005). In the Red Sea, glacial-interglacial differences in sea surface temperature were of the order of 3°–4°C (Arz et al. 2003*b*; Trommer et al. 2011), with a bias toward summer. These estimates for the Red Sea are in agreement with estimates for the western Arabian Sea (see compilation of Rohling et al. 2012).

Terrestrial temperature contrasts between glacials and interglacials are typically around 1.3 or 1.5 times larger than sea surface temperature contrasts (Braconnot et al. 2007; Laîné et al. 2009). This agrees with estimates by Kuhlemann et al. (2008) of terrestrial temperature reductions of 12°C in the northwest Mediterranean region, 7.5°C around Sicily, and 6°C or less to the south and east of Crete. Thus, mean glacial-interglacial temperature contrasts are expected on land around the Red Sea. The inferred summer bias in Arz et al. (2003*b*) and Trommer et al. (2011) suggests that the 4°–6°C contrast estimated here may also have some bias toward summer (i.e., winter contrasts may have been smaller).

A notable southward displacement of climate zones also occurred in glacials on both orbital and suborbital timescales (e.g., Wang et al. 2004, 2006), as well as global lowering of the snow line and associated vertical compression of vegetation zones (e.g., Barmawidjaja et al. 1993; Broecker and Denton 1989; Klein, Isacks, and Bloom 1995; Kuhlemann et al. 2008). Such snow line and vegetation displacements were particularly strongly expressed in the mountain ranges along the northern margin of the Mediterranean (Kuhlemann et al. 2008).

In a general sense, summer circulation/monsoons were weakened in the Northern Hemisphere during glacial periods, and winter circulation/monsoons were strengthened (e.g., Rohling, Mayewski, and Challenor 2003; Rohling et al. 2009*c* and references therein).

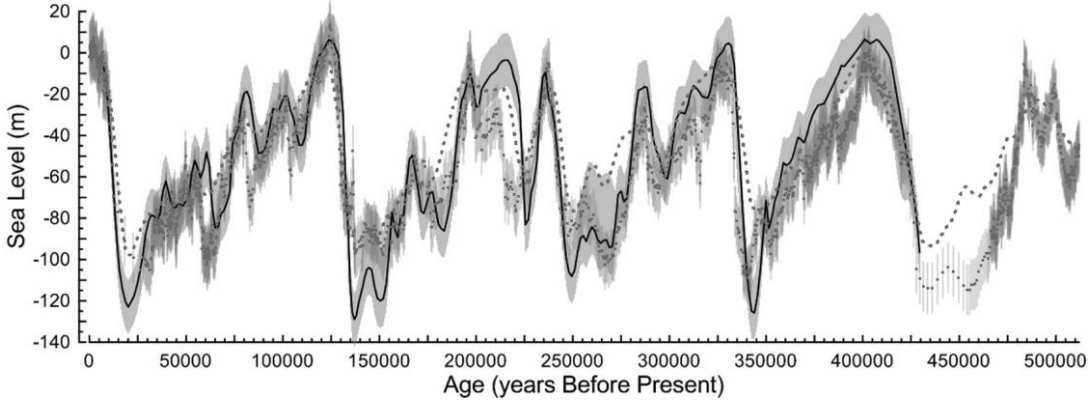

Figure 4. Comparison between three approaches for reconstructing continuous records of sea-level variations. Black is Waelbroeck et al. (2002), based on coral-calibrated deep-sea stable oxygen isotope data, with uncertainties in gray. The dashed line is the reconstruction of De Boer et al. (2010, 2011) from a model-based deconvolution of deep-sea stable oxygen isotope records into a temperature and a sea-level component following the method of Bintanja, van de Wal, and Oerlemans (2005). Dots with (2σ) uncertainty bars represent the Red Sea reconstruction on a U-Th-adjusted chronology (Rohling et al. 2009*b*, 2010). Modified after Rohling et al. (2012). A color version of this figure is available in the online edition of *Current Anthropology*.

Overall, atmospheric dust transport was strongly intensified during glacials (e.g., Lambert et al. 2008; Larrasoaña et al. 2003; Mayewski et al. 1997; Roberts et al. 2011; Rohling, Mayewski, and Challenor 2003; Ruth et al. 2007; Trauth, Larrasoaña, and Mudelsee 2009; Winckler et al. 2008), which attests to increased aridity, stronger winds, and reduced vegetation cover (reduced soil cohesion). However, even within the Mediterranean and Red Sea region, there can be considerable spatial differences in dust flux histories because of spatially different conditions in the various dust source areas. The western Mediterranean receives dust from northwest Africa/western Sahara, while the eastern Mediterranean receives dust from the eastern Sahara (Libya, Egypt). The Red Sea receives influxes of windblown dust from the easternmost Sahara, Sudan, and Saudi Arabia (Hickey and Goudie 2007; Jiang et al. 2009; Middleton and Goudie 2001; fig. 5). On millennial timescales, dust variability from various source areas varies considerably within and around the Mediterranean and Red Seas; these variations do not seem to be systematic between the two basins (Roberts et al. 2011; fig. 6). This suggests considerable regional differences in the temporal variability of vegetation cover, soil cohesion, and wind patterns/intensities.

Ice-core records from Greenland and Antarctica reveal that glacial periods were characterized by strong temperature fluctuations on millennial timescales (fig. 7). Antarctic ice-core records reveal climate variability that was less abrupt and of smaller amplitude than that observed in Greenland (Blunier et al. 1998; EPICA Community Members 2006). Continuous records of sea-level variability, developed from Red Sea oxygen isotope records, indicate that within the last glacial cycle, global ice volume fluctuated on millennial timescales with a rhythm close to that of variability observed in Antarctic climate records (Grant et al. 2012; Rohling et al. 2004*a*, 2009*b*; Siddall et al. 2003, 2008).

Greenland ice-core records and North Atlantic marine sediment records provide evidence of particularly strong climate fluctuations that have become known as Dansgaard-Oeschger cycles, which include the particularly cold Heinrich events (e.g., Broecker 2000; Dansgaard et al. 1993; Grootes et al. 1993; Hemming 2004). In many records, these millennial-scale fluctuations appear as an alternation between more intense and less intense glacial conditions, and the Heinrich events are often particularly cold/intense. Western Mediterranean sea surface temperature strongly fluctuated in close agreement with the Dansgaard-Oeschger cycles and Heinrich events (Cacho et al. 1999, 2000, 2001; Frigola et al. 2007; Martrat et al. 2004; Rohling et al. 1998*b*).

Dansgaard-Oeschger oscillations in the Northern Hemisphere were related to Antarctic (Southern Hemisphere) temperature cycles through a systematic out-of-phase relationship (e.g., Blunier and Brook 2001; Blunier et al. 1998; EPICA Community Members 2006; Stocker and Johnsen 2003). In this relationship, which has become known as the "bipolar

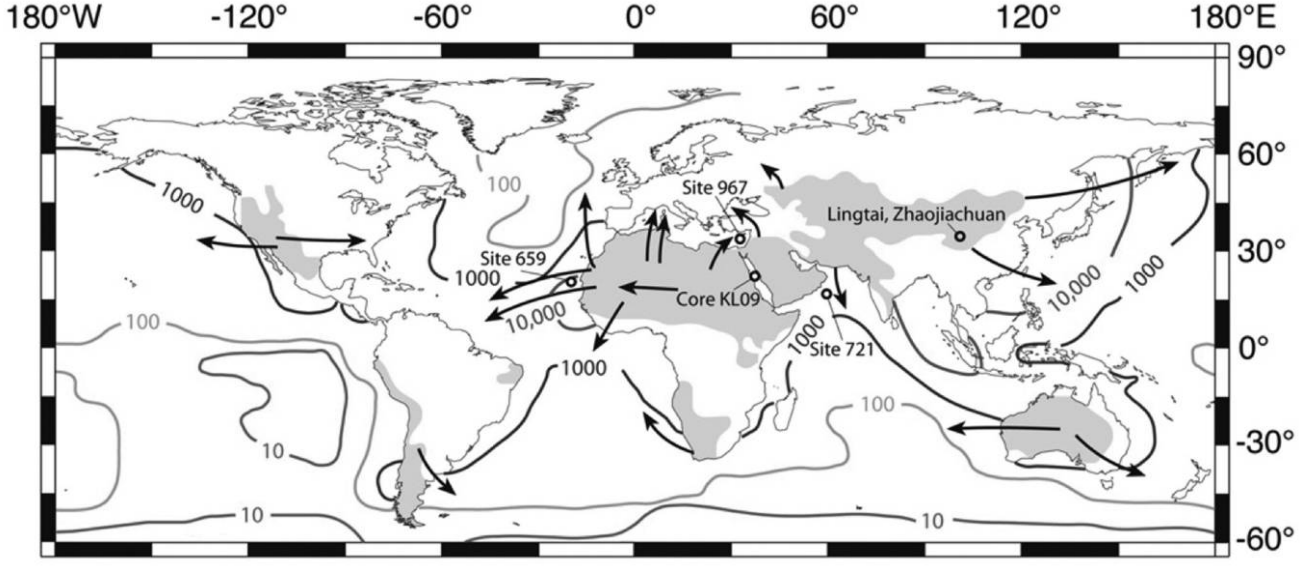

Figure 5. Major global dust sources and locations of dust records. Dust flux contours (mg m^{-2} yr^{-1}) are shown in oceans surrounding dust sources (after Duce et al. 1991). Locations of dust records discussed are indicated (ocean drilling program sites 659: Tiedemann, Sarntheim, and Shackleton 1994; 721: deMenocal, Bloemendal, and King 1991; 967: Larrasoaña et al. 2003; and the Zhaojiachuan and Lingtai loess sections: Sun et al. 2006). Site KL09 is the Red Sea record presented in Rohling et al. (2008*a*, 2009*b*) and Roberts et al. (2011). Modified after Roberts et al. (2011). A color version of this figure is available in the online edition of *Current Anthropology*.

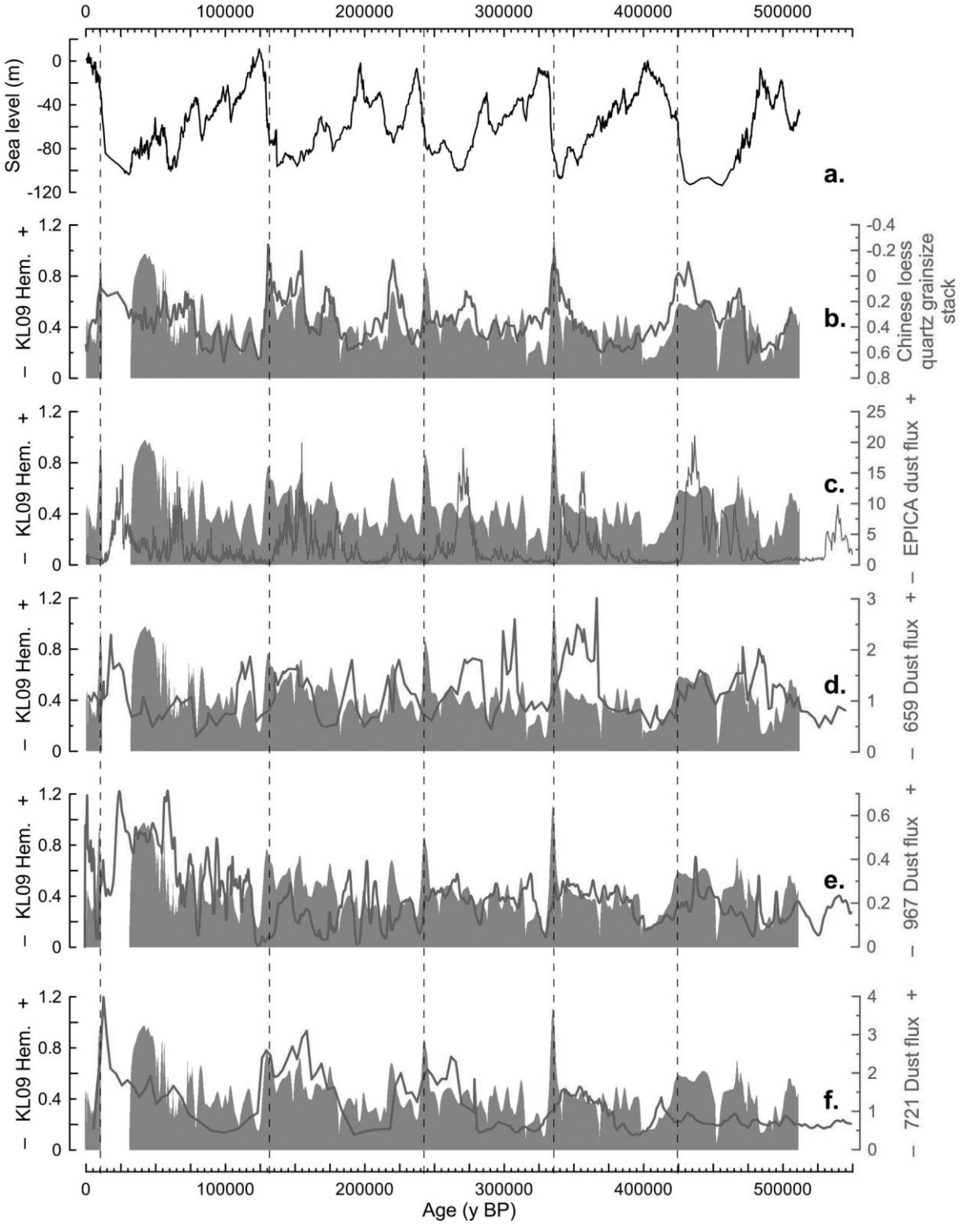

Figure 6. Comparison of sea-level and dust records for the Red Sea, circum-Sahara region, and Chinese loess plateau. *a*, Central Red Sea sea-level reconstruction (Rohling et al. 2009*b*, 2010). *b*, Environmental magnetic IRM900 mT@AF120 mT proxy for windblown hematite (Hem.) in Red Sea core KL09 (gray) compared with the stacked Chinese loess grain size record from Zhaojiachuan

temperature seesaw," the magnitude of warming in the Southern Hemisphere is proportional to the duration of cold episodes in the Northern Hemisphere (e.g., EPICA Community Members 2006; Stocker and Johnsen 2003). Siddall et al. (2010) identified during which intervals of the last 500,000 yr such millennial-scale climate variability has been particularly pronounced and found that this was the case at 480–460, 440–400, 380–360, 340–320, 260–220, 200–160, 140–120, and 80–40 ka (fig. 7). Because of the global nature of this variability, it may be expected that these intervals of generally enhanced climate variability will be noticeable in records from Africa and Eurasia even if the exact nature of the variability may differ between regions.

Northern high-latitude cooling events particularly affected the northern sectors of the Mediterranean region because of cold air outbreaks that were channeled toward the basin through gaps in the mountain ranges along its northern limits, which also triggered atmospheric instability over the Mediterranean and had implications for regional precipitation regimes (e.g., Casford et al. 2003; Frigola et al. 2007; Kuhlemann et al. 2008; Rohling et al. 1998*b*, 2002*b*). Thus, vegetation (pollen) records from the western Mediterranean and northern sector of the eastern Mediterranean also reflect the strong effects of northerly (Greenland-style) climate influences (e.g., Allen et al. 1999; Kotthoff et al. 2008; Moreno et al. 2002; Müller and Pross 2007; Sánchez-Goñi et al. 2002; Tzedakis 1999, 2009; Tzedakis et al. 2004).

From the Red Sea area, relatively little is known about climate variability. It was always dry, with high windblown dust input, but this input nevertheless reveals intensity variations that are closely similar to those observed on the Chinese loess plateau (Roberts et al. 2011). This suggests that the main climate influences over the central Red Sea (with respect to windblown dust input) were dominated by atmospheric circulation/wind changes that reflect the larger westerlies-dominated Northern Hemisphere climate variability and Indian-Asian monsoon variability (e.g., Porter and An 1995; Rohling, Mayewski, and Challenor 2003).

African Monsoon Changes

Superimposed on the glacial cycles, the entire Mediterranean region is strongly affected by monsoon intensity variations, which are dominated by Northern Hemisphere insolation changes that mainly reflect the influences of precession and eccentricity (e.g., COHMAP Members 1988; Kutzbach and Gallimore 1988; Kutzbach and Guetter 1986; Kutzbach and Street-Perrott 1985; Rossignol-Strick 1985). African monsoon maxima are well known to have been associated with insolation maxima. Freshwater flooding from the African margin into the Mediterranean during these times caused collapse of deepwater formation, eventually resulting in deepwater anoxia. These events are easily recognized in eastern Mediterranean sedimentary sequences because organic carbon preservation led to the formation of characteristic black organic rich layers, called sapropels (e.g., Rohling 1994 and references therein).

The Mediterranean sapropel record reflects the more intense African monsoon maxima, and individual sapropels have been dated (Emeis et al. 2000; Hilgen 1991; Hilgen et al. 1993; Kroon et al. 1998; Lourens, Wehausen, and Brumsack 2001; Lourens et al. 1996) based on the ages of precession-driven insolation maxima that are known from astronomical solutions (Berger 1977; Laskar et al. 2004; Milankovitch 1941). A particularly straightforward summary table of ages is given for the main sapropels by Kroon et al. (1998), after Lourens et al. (1996). These datings may be important for archaeological, anthropological, and biogeographical studies because they provide a chronological framework that may help us to date and understand, for example, past migration pulses through the Sahara desert region (e.g., Drake et al. 2011; Osborne et al. 2008) or past humid phases associated with fossil hominid finds (e.g., Brown, McDougall, and Fleagle 2012; McDougall, Brown, and Fleagle 2005, 2008). The sapropel record indicates that there have been more than a hundred of such strongly developed African monsoon maxima over the past couple of million years (Larrasoaña, Roberts, and Rohling 2013).

During times with intensified African monsoon circulation, the spatial extent of the Sahara Desert was much reduced, which has become known as "greening of the Sahara," when the African monsoon penetrated farther northward than today (Larrasoaña, Roberts, and Rohling 2013). This penetration was partly due to orbital forcing and partly resulted from northward expansion of vegetation into the previously more reflective desert, which in turn triggered further northward penetration of the monsoon front in a "vegetation-albedo feedback process" (e.g., Brovkin et al. 1998; Claussen et al. 1998; Foley et al. 2003). During intense monsoon maxima,

and Lingtai, Chinese loess plateau (from Sun et al. 2006, with minor age adjustments in Roberts et al. 2011). *c*, *d*, *e*, and *f*, respectively, compare the Red Sea dust record (gray) with dust records from EPICA Dome C, Antarctica (Lambert et al. 2008); ODP Site 659, off northwest Africa (Tiedemann, Sarntheim, and Shackleton 1994); ODP Site 967, eastern Mediterranean Sea (Larrasoaña et al. 2003); and ODP Site 721, Arabian Sea (deMenocal, Bloemendal, and King 1991). Vertical dashed lines coincide with Red Sea dust peaks at the glacial terminations and are shown to assist comparisons between panels. The Red Sea records are shown for consistency on the same chronology (Rohling et al. 2009*b*, 2010) as used in Roberts et al. (2011). This chronology is (subtly) updated within the last 150,000 yr in figures 7 and 8 based on the latest age controls developed by Grant et al. (2012). A color version of this figure is available in the online edition of *Current Anthropology*.

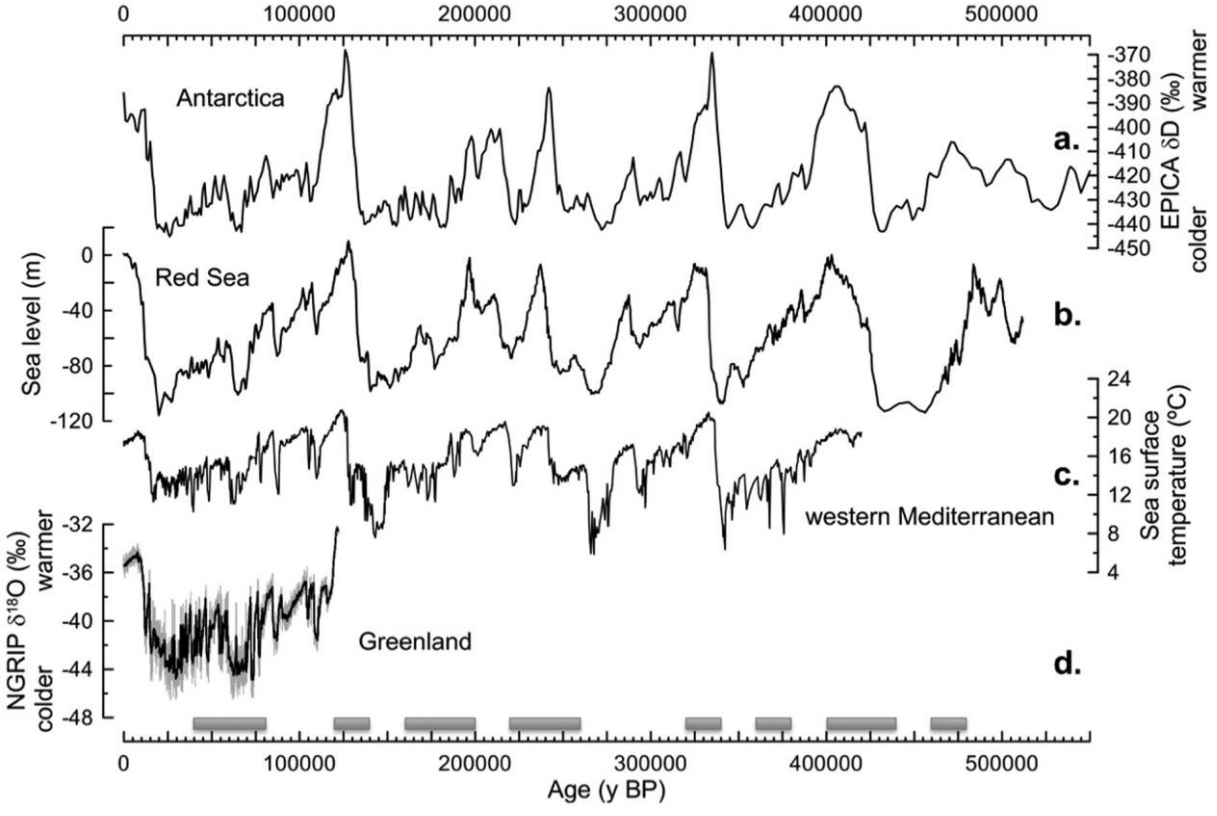

Figure 7. Comparison of different records of climate variability including polar ice-core records, sea level, and Mediterranean temperature variability. *a*, EPICA Dome C ice-core stable hydrogen isotope proxy for temperature, Antarctica (Jouzel et al. 2007). *b*, The Red Sea sea-level record in the pre-150 ka interval on the chronology of Rohling et al. (2009*b*, 2010) and in the post-150 ka interval on the latest chronology using the age constraints developed by Grant et al. (2012). *c*, Sea surface temperature in the Alboran Sea, westernmost Mediterranean (Martrat et al. 2004). *d*, Stacked North-GRIP ice-core oxygen isotope proxy for temperature, Greenland (gray; Wolff et al. 2010), and—for clarity—a 21-point moving average smoothing (black). Bars at the bottom indicate intervals of particularly pronounced millennial-scale climate variability after the analysis of Siddall et al. (2010). A color version of this figure is available in the online edition of *Current Anthropology*.

the monsoon front appears to have penetrated northward past the central Saharan watershed (at about 21°N), and seasonal runoff occurred from the central Saharan mountains into the eastern Mediterranean along the wider North African margin (Drake et al. 2011; Osborne et al. 2008; Paillou et al. 2009; Rohling et al. 2002*a*, 2004*a*, 2004*b*). Such drainages will have presented green corridors along which humans and animals may have migrated across the otherwise arid region (Drake et al. 2011; Osborne et al. 2008). These ideas integrate a wide variety of evidence for past increases in precipitation and water availability throughout the currently hyperarid Sahara, including the distributions of animal and human fossils, sedimentological data, lake-level reconstructions, etc. (e.g., Armitage et al. 2007; Cremaschi 2002; Drake et al. 2011; Gasse 2000; Gaven et al. 1981; Kuper and Kröpelin 2006; Larrasoaña, Roberts, and Rohling 2013; Mandell and Simmons 2001; Pachur 2001; Pachur and Altmann 2006; Pachur and Braun 1980; Szabo, Haynes, and Maxwell 1995). Records of African monsoon variability reveal that centennial- to millennial-scale decreases/collapses in monsoon intensity occurred during several monsoon maxima and that these roughly coincided with intrusions of northerly cooling events into the Mediterranean basin (e.g., Casford et al. 2003; Gasse 2000; Mercone et al. 2001; Osborne et al. 2008; Rohling et al. 2002*a*, 2002*b*, 2004*b*; Scrivner, Vance, and Rohling 2004).

It is important to note that there is no evidence that the African monsoon penetrated at any time directly into the Mediterranean basin. Rainfall gradient and isotope reconstructions in the Levant indicate that rain in that region was always sourced from the north and west, from the Mediterranean, even during monsoon maxima (Bar-Matthews et al. 2003; Goodfriend 1991; Matthews, Ayalon, and Bar-Matthews 2000; McGarry et al. 2004; Vaks et al. 2007). Moreover, Tzedakis (2009) presented a compelling case that times of insolation-driven African monsoon maxima were not characterized by enhanced summer precipitation around the northern and eastern Mediterranean, as had been often suggested before (e.g., Rohling and Hilgen 1991; Tzedakis 2009;

and references therein). Pollen data indicate that summer aridity was enhanced at these times and that any enhanced rainfall likely took place in winter (with some possible regional exceptions); that is, typical Mediterranean climate conditions were intensified (Tzedakis 2009).

During opposite phases of the precession cycle, the monsoon was weak, and the (hyper)arid Sahara desert was spatially extended, similar to the present, without watercourses crossing it to the wider North African margin. Orbital cyclicity in the African monsoon is obvious in records of windblown dust fluxes from the Sahara (e.g., Larrasoaña et al. 2003; Lourens, Wehausen, and Brumsack 2001; Trauth, Larrasoaña, Mudelsee 2009; Wehausen and Brumsack 2000), which reflects insolation forcing of the African monsoon.

Indian Monsoon Changes

Variations in the Indian Ocean monsoon circulation, which affect the wind field over the southern sector of the Red Sea region, have been documented especially by marine sedimentary records from the Arabian Sea (e.g., Almogi-Labin et al. 2000; Clemens and Prell 1990, 2003; Clemens et al. 1991; Ivanochko et al. 2005; Prell and Kutzbach 1987; Reichart, Lourens, Zachariasse 1998; Rostek et al. 1997; Schmiedl and Leuschner 2005; Schultz, von Rad, and Erlenkeuser 1998; Sirocko et al. 1993) and by speleothem records from Oman and Socotra (Burns et al. 2003, 2004; Fleitmann et al. 2003*a*, 2003*b*, 2004, 2007). Long Arabian Sea records provide convincing evidence for a predominant control of orbital precession and thus insolation on the Indian monsoon intensity, similar to the African monsoon. Speleothem data from Oman (Fleitmann et al. 2003*a*, 2003*b*, 2004, 2007) indicate that the precipitation regime of the Indian Ocean monsoon expanded to affect the southeastern margin of the Arabian Peninsula during the Early to Middle Holocene summer southwest Monsoon maximum, whereas that region currently (during the opposite precession phase) is unaffected (Conroy and Overpeck 2011).

Trommer et al. (2011) described the timing of a somewhat more humid interval in the central Red Sea Bakala (Tokar) wadi catchment and found that this started immediately following the last interglacial sea-level highstand and lasted several thousand years. This relative timing agrees with the period of deposition of the deep-sea anoxic event known as sapropel S5 in the eastern Mediterranean (Grant et al. 2012), which is also recognized as a humid interval in the speleothem record of Soreq cave, Israel, which reflects the last interglacial African monsoon maximum (Bar-Matthews, Ayalon, and Kaufman 1997, 2000; Bar-Matthews et al. 1999, 2003). U-series dating of the Soreq cave record demonstrates that the last interglacial African monsoon maximum dates to 128–120 ka. This agrees with datings from Dongge cave, China, for the last interglacial maximum of the Asian monsoon, from 129.3 $\pm$ 0.9 to 119.6 $\pm$ 0.6 ka (Yuan et al. 2004). On millennial scales, therefore, the timing of monsoon maxima seems to be roughly similar for all three major monsoon systems (African, Indian, and Southeast Asian).

Red Sea records contain no evidence for any major precipitation/vegetation changes associated with monsoon maxima; the area appears to have remained (hyper)arid. Monsoon variability, however, affected Red Sea oceanography through changes in the wind field over the basin (Biton et al. 2010; Trommer et al. 2011), and strong windblown dust variations over time support the notion of important fluctuations in wind forcing over the basin (Roberts et al. 2011; Rohling et al. 2008*a*).

Millennial-scale variability in windblown dust records of the central Red Sea is coherent with millennial-scale changes in Arabian Sea productivity (Rohling et al. 2008*a*; Schultz, von Rad, Erlenkeuser 1998) as well as with Chinese loess records (Porter and An 1995; Roberts et al. 2011; Sun et al. 2006). This links Arabia with winter-dominated climate variability as recorded in Greenland ice-core records (Rohling, Mayewski, and Challenor 2003). In short, there is good evidence that colder conditions in Greenland coincided with intensified winter-type atmospheric circulation over Asia, which also affected Arabia, possibly through the winter (northeast) monsoon.

Implications and Conclusions

Conditions Relevant to Proposed Migration Routes across the Southern Red Sea

Sea level. The intense ice-age cycles of the last 500,000 yr have been associated with important variability in global sea level over a range of 120 m or more below the present to perhaps 10 m above the present (fig. 4). The Strait of Bab-el-Mandab in the southern Red Sea, which connects the basin with the open ocean, is highly sensitive to sea-level change because it is (today) only 137 m deep. This is of the same order as past sea-level drops during glacial maxima, and there have consequently been many proposals of a potential migration route across the southern Red Sea, assuming that a passage between Africa and Arabia may have emerged during times of maximum glacial sea-level lowstands.

Fernandes, Rohling, and Siddall (2006) evaluated the concept of emergence of a southern land bridge between Africa and Arabia and concluded that there is no evidence for it at any time during the last 500,000 yr. Emergence of a land bridge in the strait would rapidly lead to desiccation within the highly evaporative Red Sea, with deposition of evaporites within a matter of several centuries in the open basin and within a matter of years to decades in shallow coastal environments. Moreover, there is evidence of substantial persistent local water depths above the sill in the strait of at least 15 m (Fernandes, Rohling, and Siddall 2006) and up to 35 m (Biton, Gildor, and Peltier 2008); for the Last Glacial Maximum, the passage depth has been estimated as up to 25 $\pm$ 4 m (Lambeck et al. 2011). For lower water depths, inflow from the open

ocean would have become sufficiently restricted for basin-wide development of extreme salinities in excess of about 75 practical salinity units (psu). There is evidence that salinities at times rose above 49 psu, causing local extinction of planktonic foraminifera (Fenton et al. 2000 and references therein). However, salinities remained below 75 psu given that higher values would have also caused the local extinction of all pteropods and all benthic foraminifera, which did not happen (Fenton et al. 2000; Rohling et al. 1998*a*).

Regardless of the above, the strait passage was much shallower and narrower than today during glacial sea-level lowstands (Lambeck et al. 2011; Rohling et al. 1998*a*; Siddall et al. 2004). This is especially clearly illustrated by a recent advanced reconstruction of strait morphology during the Last Glacial Maximum (Lambeck et al. 2011), which takes into account detailed hydrographic data for the present-day strait, sea-level change during the Last Glacial Maximum, and a model for isostatic change components. Lambeck et al. (2011) also present arguments about older glacial lowstands and support the notion that an open passage remained in existence. In summary, it is evident from the combined studies that any migration across the southern Red Sea during glacial sea-level lowstands would have (*a*) benefited from the fact that the marine passage was strongly reduced in width, and (*b*) definitely included some element of swimming, rafting, or navigation.

Climate conditions. Another important control on potential migrations across the southern Red Sea concerns regional climatic conditions. For example, was enough water and food available to sustain migrating animals/humans on either side of the strait? This question has come to the fore because of a recent proposal (Armitage et al. 2011) that an early wave of human migration out of Africa occurred across the southern Red Sea, with migration toward and across the strait region during the penultimate glacial maximum (the "Saalian") and subsequent spreading across/along the Arabian Peninsula during the monsoon maximum of the last interglacial (about 128–120 ka).

Red Sea sedimentary records provide important insights into regional climatic conditions. Windblown dust concentrations have been measured in exactly the same sedimentary sequences that were used to reconstruct the Red Sea sea-level record. This dust record clearly illustrates that the transition between the Saalian glacial and the last interglacial was characterized by extreme fluxes of windblown dust, which reflect high winds and pronounced aridity in the region (Roberts et al. 2011). Organic geochemical data, also from the same sample sequence, demonstrate that (lightly) enhanced humidity in the Red Sea region—the most likely local expression of the last interglacial summer monsoon maximum—first developed only after the sea-level highstand had peaked and sea level had started to drop again (Trommer et al. 2011). Data from Oman suggest that relatively more humid conditions may have started to develop earlier, from about 135 ka (Fleitmann et al. 2003*b*; Vaks et al. 2007), a little later than in the eastern Sahara (from 140 ka; Osmond and Dabous 2004; Szabo, Haynes, and Maxwell 1995; Vaks et al. 2007).

It would be an oversimplification to assume a simple succession from low sea level to favorable climate for migration across the Arabian Peninsula during the transition from the Saalian glacial to the last interglacial. The data instead reveal considerable complexity across that transition, highlighting that the sea-level lowstand and the climatically more favorable conditions were separated by at least 5,000 yr of arid regional conditions and sharp sea-level rise (Roberts et al. 2011). This does not exclude the possibility that the southern route out of Africa was employed at this time. But if it was, then the animals/humans involved must have been resilient to significantly adverse environmental conditions. We note that a similar sequence of events is observed for almost all glacial terminations. In the next section, we elaborate a new view of more promising migration intervals.

A new concept: "windows of opportunity" for southern migration out of Africa. Our sea-level and windblown dust records, sampled from the same central Red Sea sediment sequence (Rohling et al. 2008*a*, 2009*b*, 2010; Roberts et al. 2011) are shown in figure 8. The last 150,000 yr are shown on a new chronology (Grant et al. 2012, which is tightly constrained relative to the U-Th dated Soreq Cave record from Israel; Bar-Matthews, Ayalon, and Kaufman 1997; Bar-Matthews et al. 1999, 2000, 2003). Before 150 ka, the records are shown on a chronology developed (Rohling et al. 2009*b*) by correlation with the European Project for Ice Coring in Antarctica (EPICA) Dome C temperature proxy record on the EDC3 chronology (Jouzel et al. 2007) with an adjustment that accounts for radiometric datings of past sea-level highstands (Rohling et al. 2010).

The horizontal light gray bar in figure 8 highlights relatively low dust fluxes similar to those of the Holocene. During times with such relatively low dust fluxes, we suggest that the regional climate may have been most favorable for habitation/migration in contrast to the intervening intervals with high dust fluxes, which attest to more intense winds and lower soil cohesion due to even lower soil moisture and even more scarce vegetation cover than today. The vertical light gray bars identify periods when both (*a*) sea level stood 100 m or more below the present, so that the marine connection to be crossed in the Strait of Bab el Mandab would have been only some 6 km wide (cf. Last Glacial Maximum reconstruction of Lambeck et al. 2011); and (*b*) dust fluxes were relatively low. These highlighted intervals therefore represent periods with relatively favorable conditions (windows of opportunity) for potential migrations between northeast Africa and southwest Arabia via a southern route. There is increasing evidence that the southern route was used for the final migration out of Africa by AMHs (e.g., Derricourt 2005; Fernandes et al. 2012).

The highlighted periods of significant sea-level lowstands were also characterized by emerged continental shelves

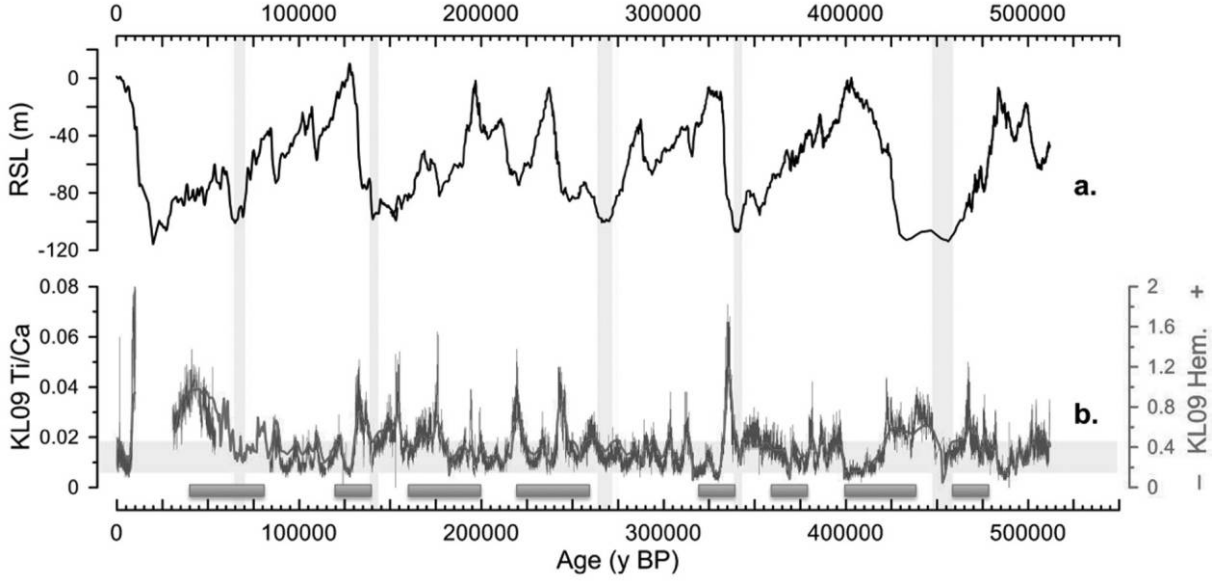

Figure 8. Direct comparison between (*a*) the latest version of the Red Sea sea-level reconstruction, with the pre-150 ka interval on the chronology of Rohling et al. (2009*b*, 2010) and the post-150 ka interval on the new chronology of Grant et al. (2012), and (*b*) central Red Sea dust proxy data, including the Ti/Ca ratio from core-scanning XRF analysis (gray) and hematite concentration data from environmental magnetic analyses (smooth line; see also Roberts et al. 2011; Rohling et al. 2008*a*). Data originate from a single sampling of the same sedimentary sequence, which ensures unambiguous phase relationships between the various records. Light gray bars are explained in the text. Horizontal bars at bottom indicate intervals of particularly pronounced millennial-scale climate variability, after the analysis of Siddall et al. (2010; see also fig. 7). A color version of this figure is available in the online edition of *Current Anthropology*.

around the Arabian Peninsula. These provided excellent habitation and migration potential for animals and humans, especially if the enhanced hydraulic head due to sea-level lowering led to enhanced freshwater seepage on the emerged shelves from groundwater reservoirs (e.g., Parker and Rose 2008). Such seepage exists even today on the shelves, in submarine form (Ghoneim 2008; Parker and Rose 2008). The emerged shelves may therefore have presented an excellent habitat with gentle topography, freshwater availability, and an abundance of coastal/marine resources. If emerged shelves were key migration/habitation zones, then much of the anthropological record may now be under water.

Several windows of opportunity for migration along the southern route out of Africa within the last half-million years are highlighted in figure 8. These windows date to about 458–448, 345–340, 272–265, 145–140, and 70–65 ka. The interval of 145–140 ka may be relevant with respect to a tentative early migration of AMHs that led to early inhabitation at the Hormuz region of the Arabian Gulf with an oldest dating of 127 ± 16 ka (Armitage et al. 2011). That population is thought to have been "unsuccessful" in that it did not leave any descendants (Fernandes et al. 2012). Instead, all non-African humans originate from a more recent migration out of Africa dated with various molecular clock approaches at around 57–65 ka, with an upper age bound of 70–65 ka based on East African data (Fernandes et al. 2012). This age range of 65 +5/−8 ka is in remarkable agreement with our window of opportunity of 70–65 ka for a southern route migration out of Africa. The chronological uncertainties for our records in that interval are less than 1,000 yr (Grant et al. 2012). Haplotype dispersal maps suggest that the migration at around 65 ka followed the southern route out of Africa and that Arabia was the first staging post in the spread of AMHs around the world (Fernandes et al. 2012).

Conditions Relevant to Habitation of and Migration through the Sahara

Migration potential through the Sahara Desert was comprehensively assessed by Drake et al. (2011). Their abstract says it all:

> Both animals and humans populated it [the Sahara] during past humid phases. . . . More animals crossed via this route than used the Nile corridor . . . [and] many of these species are aquatic. This dispersal was possible because during the Holocene humid period the region contained a series of linked lakes, rivers, and inland deltas comprising a large interlinked waterway, channeling water and animals into and across the Sahara. . . . This system was last active in the early Holocene when many species appear to have occupied the entire Sahara. Human dispersals were influenced by this distribution. . . . Lacustrine sediments show that the

> "green Sahara" also existed during the last interglacial (~125 ka) and provided green corridors that could have formed dispersal routes at a likely time for the migration of modern humans out of Africa.

Both periods highlighted in that study are well-known insolation-driven African monsoon maxima. The Holocene period is known to correspond to eastern Mediterranean sapropel S1 and the last interglacial period to sapropel S5 (e.g., Larrasoaña, Roberts, and Rohling 2013; Osborne et al. 2008; Rohling and Hilgen 1991; Rohling et al. 2002*a*, 2004*b*; Scrivner, Vance, and Rohling 2004).

Archaeological observations around exclusively rain-fed depressions on the Libyan Plateau suggest that monsoonal summer rains from central Africa periodically penetrated at least as far north as Kharga (roughly 25°N) during the Holocene monsoon maximum despite the fact that conditions during that pluvial phase seem to have remained drier than during earlier Quaternary pluvial phases (Mandel and Simmons 2001). This suggestion that the Holocene monsoon maximum was of a relatively low intensity compared with previous Quaternary monsoon maxima has been corroborated by quantitative reconstructions of effects of the Holocene and last interglacial monsoon maxima in the eastern Mediterranean (Rohling 1999; Rohling et al. 2004*b*). Hence, past monsoon maxima—datings for which can be obtained from the astronomical ages of insolation-driven monsoon maxima (Emeis et al. 2000; Hilgen 1991; Hilgen et al. 1993; Kroon et al. 1998; Lourens et al. 1996, 2001)—represent times of enhanced humidity that may have been crucial for migrations through the otherwise hyperarid Sahara "barrier" between sub-Saharan Africa and the Mediterranean/Levantine regions (Larrasoaña, Roberts, and Rohling 2013).

As mentioned above, several African monsoon maxima (e.g., the Holocene and last interglacial) have been interrupted by centennial- to millennial-scale periods of reduced monsoon intensity. Hence, potential routes for migration through the Sahara region remained intermittent, subject to periodic returns of harsh conditions.

Finally, hypotheses that invoke an importance of periods of rapid, millennial-scale climate variability for developments and/or migrations of hominins and their food sources—for example, through intermittent habitat fragmentation—may benefit from the objectively identified episodes of generally (globally) enhanced millennial-scale climate variability (Siddall et al. 2010). We have indicated these intervals (480–460, 440–400, 380–360, 340–320, 260–220, 200–160, 140–120, and 80–40 ka) in figures 7 and 8.

Conditions Relevant to Migrations through the Levant

Conditions for migrations through the Levant are normally poor because of hyperarid conditions in the Sinai-Negev region. However, data from a north–south array of caves highlight a window of time between 140 and 110 ka when this region was intermittently more humid (especially between 133 and 122 ka) and thus more hospitable (Vaks et al. 2007). This closely matches data that indicate more humid conditions in the Egyptian Sahara (Osmond and Dabous 2004), which suggests a high probability that a pathway existed through the Levant for migrations out of Africa between about 140 and 110 ka, with possible extension to 85 ka, after which hyperarid conditions were reestablished (Vaks et al. 2007).

Derricourt (2005) reviewed climatic and archaeological studies to conclude that the Levantine route was the most likely route of early (pre-85 ka) migrations out of Africa in contrast to the youngest (post-85 ka) migration, which he links more to a southern route across the Bab-el-Mandab Strait (see above). Early AMH finds from Qafzeh and Skhul in the Near East date to between 119 ± 18 and 81 ± 13 ka (e.g., Armitage et al. 2011; Grün et al. 2005; Petraglia 2011; Shea 2008). Genetic data indicate that this migration did not leave any descendants in the modern human population outside Africa, which instead can be traced back to a migration out of Africa that took place around 65 ka, likely via a southern route (Fernandes et al. 2012; see above).

For Levantine migration routes, the key control may have been exerted by development of pluvial episodes as recorded and accurately dated in cave speleothem deposits (e.g., Derricourt 2005; Shea 2008; Vaks et al. 2007). These intermittently more humid conditions in the Levant are closely related to monsoon maxima associated with Northern Hemisphere insolation maxima. It should be emphasized that monsoon maxima, with "greening of the Sahara," were not limited to only interglacial insolation maxima but occurred also during insolation maxima within glacial times (e.g., Larrasoaña, Roberts, and Rohling 2013; Larrasoaña et al. 2003; Liu et al. 2012).

The control by pluvials that applies to the Levantine route is considerably more straightforward than the windows of opportunity control we have proposed in "A new concept: 'windows of opportunity' for southern migration out of Africa" for the southern route, which requires a combination of low sea level and concomitant interludes of relatively favorable climate conditions. These windows of opportunity are not simply aligned with monsoon maxima but instead reflect millennial-scale episodes of relatively favorable climate within glacial maxima.

Conditions along the European Margin of the Mediterranean

As recorded in Greenland ice cores, the European margin of the Mediterranean has been strongly affected by intense climate swings that originate in the North Atlantic region. Cold events were transmitted to the Mediterranean by northerly air outbreaks through gaps in the mountainous topography around the northern margin of the Mediterranean, especially over the northwest Mediterranean, the Adriatic Sea, and the Aegean (e.g., Casford et al. 2003; Frigola et al. 2007; Kuhlemann et al. 2008; Moreno et al. 2002; Rohling et al. 1998*b*, 2002*b*). During the Holocene, a strong temporal coincidence

has been found between the northerly cooling events and archaeological transitions in the northeastern sector of the Mediterranean region (Clare et al. 2008). Because of resultant atmospheric instabilities within the Mediterranean basin, northerly cooling events may have had an amplified effect on snow line lowerings and vegetation-zone migrations in the Mediterranean region (e.g., Kuhlemann et al. 2008 and references therein).

Despite this glacial variability, the Mediterranean region during glacial times was a refugium with relatively mild conditions for plants and animals, avoiding the much more severe climatic stress over the main Eurasian landmass to the north of the Alps/Carpathians (e.g., Blondel 2009; Tzedakis 2009). The region's great diversity of terrain and microclimates, drainage patterns, and accentuated relief with many rock shelters and caves would have been conducive to a relatively rich variety of exploitable plant and animal food sources and to camp locations. From a climatic point of view, therefore, it is likely that habitation and migration were possible throughout this region even during severe glacials, especially in lowlands and coastal plains, and that there was the potential to range into higher elevations during periods with milder conditions.

Acknowledgments

Thanks to the Wenner-Gren Foundation for organizing the conference and arranging for publication of the papers presented there and to Erella Hovers and Steve Kuhn and two anonymous reviewers for their constructive assessments of earlier versions of the manuscript. This paper contributes to the United Kingdom Natural Environment Research Council projects NE/E01531X/1 (RESET), NE/I009906/1 (iGlass), and NE/H004424/1 as well as E. J. Rohling's Royal Society–Wolfson Research Merit Award and Australian Laureate Fellowship FL120100050.

References Cited

Adamson, D. A., F. Gasse, F. A. Street, and M. A. J. Williams. 1980. Late Quaternary history of the Nile. *Nature* 288:50–55.

Allen, J. R. M., U. Brandt, A. Brauer, H. W. Hubberten, B. Huntley, J. Keller, M. Kraml, et al. 1999. Rapid environmental changes in southern Europe during the last glacial period. *Nature* 400:740–743.

Almogi-Labin, A., G. Schmiedl, C. Hemleben, R. Siman-Tov, M. Segl, and D. Meischner. 2000. The influence of the NE winter monsoon on productivity changes in the Gulf of Aden, NW Arabian Sea, during the last 530 ka as recorded by benthic foraminifera. *Marine Micropaleontology* 40:295–319.

Armitage, S. J., N. A. Drake, S. Stokes, A. El-Hawat, M. Salem, K. White, P. Turner, and S. J. McLaren. 2007. Multiple phases of North African humidity recorded in lacustrine sediments from the Fazzan Basin, Libyan Sahara. *Quaternary Geochronology* 2:181–186.

Armitage, S. J., S. A. Jasim, A. E. Marks, A. G. Parker, V. I. Usik, and H. P. Uerpmann. 2011. The southern route "Out of Africa": evidence for an early expansion of modern humans into Arabia. *Science* 331:453–456.

Arz, H. W., F. Lamy, J. Pätzold, P. J. Müller, and M. Prins. 2003*a*. Mediterranean moisture source for an Early-Holocene humid period in the Northern Red Sea. *Science* 300:118–121.

Arz, H. W., J. Pätzold, P. J. Müller, and M. O. Moammar. 2003*b*. Influence of Northern Hemisphere climate and global sea level rise on the restricted Red Sea marine environment during termination I. *Paleoceanography* 18: 1053, doi:10.1029/2002PA000864.

Bar-Matthews, M., A. Ayalon, M. Gilmour, A. Matthews, and C. J. Hawkesworth. 2003. Sea-land oxygen isotopic relationships from planktonic foraminifera and speleothems in the Eastern Mediterranean region and their implication for paleorainfall during interglacial intervals. *Geochimica et Cosmochimica Acta* 67:3181–3199.

Bar-Matthews, M., A. Ayalon, and A. Kaufman. 1997. Late Quaternary paleoclimate in the eastern Mediterranean region from stable isotope analysis of speleothems at Soreq Cave, Israel. *Quaternary Research* 47:155–168.

———. 2000. Timing and hydrological conditions of sapropel events in the Eastern Mediterranean, as evident from speleothems, Soreq Cave, Israel. *Chemical Geology* 169:145–156.

Bar-Matthews, M., A. Ayalon, A. Kaufman, and G. J. Wasserburg. 1999. The Eastern Mediterranean paleoclimate as a reflection of regional events: Soreq Cave, Israel. *Earth and Planetary Science Letters* 166:85–95.

Barmawidjaja, D. M., E. J. Rohling, W. A. Van der Kaars, C. Vergnaud-Grazzini, and W. J. Zachariasse. 1993. Glacial conditions in the northern Molucca Sea region (Indonesia). *Palaeogeography, Palaeoclimatology, Palaeoecology* 101:147–167.

Berger, A. 1977. Support for the astronomical theory of climatic change. *Nature* 268:44–45.

Béthoux, J. P. 1984. Paleo-hydrologie de la Mer Mediterranee au cours des derniers 20 000 ans. *Oceanologica Acta* 7:43–48.

Béthoux, J. P., and B. Gentili. 1994. The Mediterranean Sea: a test area for marine and climatic interactions. In *Ocean processes in climate dynamics: global and Mediterranean examples*. P. Malanotte-Rizzoli and A. R. Robinson, eds. Pp. 239–254. Dordrecht: Kluwer.

Bintanja, R., R. S. W. van de Wal, and J. Oerlemans. 2005. Modelled atmospheric temperatures and global sea levels over the past million years. *Nature* 437:125–128.

Biton, E., H. Gildor, and W. R. Peltier. 2008. Relative sea level reduction at the Red Sea during the Last Glacial Maximum. *Paleoceanography* 23:PA1214, doi:10.1029/2007PA001431.

Biton, E., H. Gildor, G. Trommer, M. Siccha, M. Kucera, M. T. J. van der Meer, and S. Schouten. 2010. Sensitivity of Red Sea circulation to monsoonal variability during the Holocene: an integrated data and modeling study. *Paleoceanography* 25:PA4209, doi:10.1029/2009PA001876.

Blondel, J. 2009. The nature and origin of the vertebrate fauna. In *The physical geography of the Mediterranean*. J. C. Woodward, ed. Pp. 139–163. Oxford: Oxford University Press.

Blunier, T., and E. Brook. 2001. Timing of millennial-scale climate change in Antarctica and Greenland during the last glacial period. *Science* 291:109–112.

Blunier, T., J. Chapellaz, J. Schwander, A. Dällenbach, B. Stauffer, T. F. Stocker, D. Raynaud, et al. 1998. Asynchrony of antarctic and Greenland climate change during the last glacial period. *Nature* 394:739–743.

Boucher, K. 1975. *Global climate*. London: English University Press.

Braconnot, P., B. Otto-Bliesner, S. Harrison, S. Joussaume, J. Y. Peterchmitt, A. Abe-Ouchi, M. Crucifix, et al. 2007. Results of PMIP2 coupled simulations of the mid-Holocene and Last Glacial Maximum. 1. Experiments and large-scale features. *Climate of the Past* 3:261–277.

Broecker, W. S. 2000. Abrupt climate change: causal constraints provided by the paleoclimate record. *Earth-Science Reviews* 51:137–154.

Broecker, W. S., and G. H. Denton. 1989. The role of ocean-atmosphere reorganizations in glacial cycles. *Geochimica et Cosmochimica Acta* 53:2465–2501.

Brovkin, V., M. Claussen, V. Petoukhov, and A. Ganopolski. 1998. On the stability of the atmosphere-vegetation system in the Sahara/Sahel region. *Journal of Geophysical Research* 103:31613–31624.

Brown, F. H., I. McDougall, and J. G. Fleagle. 2012. Correlation of the KHS Tuff of the Kibish Formation to volcanic ash layers at other sites, and the age of early *Homo sapiens* (Omo I and Omo II). *Journal of Human Evolution* 63:577–585.

Burns, S. J., D. Fleitmann, A. Matter, J. Kramers, and A. A. Al-Subbary. 2003. Indian Ocean climate and an absolute chronology over Dansgaard/Oeschger events 9 to 13. *Science* 301:1365–1367.

———. 2004. Indian Ocean climate and an absolute chronology over Dansgaard/Oeschger events 9 to 13: correction. *Science* 305:1567.

Cacho, I., J. O. Grimalt, M. Canals, L. Sbaffi, N. J. Shackleton, J. Schönfeld, and R. Zahn. 2001. Variability of the western Mediterranean Sea surface temperatures during the last 25,000 years and its connection with the Northern Hemisphere climatic changes. *Paleoceanography* 16:40–52.

Cacho, I., J. O. Grimalt, C. Pelejero, M. Canals, F. J. Sierro, J. A. Flores, and N. J. Shackleton. 1999. Dansgaard-Oeschger and Heinrich event imprints in Alboran Sea paleotemperatures. *Paleoceanography* 14:698–705.

Cacho, I., J. O. Grimalt, F. J. Sierro, N. J. Shackleton, and M. Canals. 2000. Evidence of enhanced Mediterranean thermohaline circulation during rapid climate coolings. *Earth and Planetary Science Letters* 183:417–429.

Cantu, V. 1977. The climate of Italy. In *Climates of central and southern Europe*. C. C. Wallen, ed. Pp. 127–183. World Survey of Climatology, vol. 6. Amsterdam: Elsevier.

Casford, J. S. L., E. J. Rohling, R. H. Abu-Zied, F. J. Jorissen, M. Leng, and J. Thomson. 2003. A dynamic concept for eastern Mediterranean circulation and oxygenation during sapropel formation. *Palaeogeography, Palaeoclimatology, Palaeoecology* 190:103–119.

Clare, L., E. J. Rohling, B. Weninger, and J. Hilpert. 2008. Warfare in Late Neolithic/Early Chalcolithic Pisidia, southwestern Turkey: climate induced social unrest in the late 7th millennium cal BC. *Documenta Praehistorica* 35:65–92.

Claussen, M., V. Brovkin, A. Ganopolski, C. Kubatski, and V. Petoukhov. 1998. Modelling global terrestrial vegetation-climate interaction. *Philosophical Transactions of the Royal Society B* 353:53–63.

Clemens, S. C., and W. L. Prell. 1990. Late Pleistocene variability of Arabian Sea summer monsoon winds and continental aridity: eolian records from the lithogenic component of deep-sea sediments. *Paleoceanography* 5:109–145.

———. 2003. A 350,000 year summer-monsoon multi-proxy stack from the Owen Ridge, northern Arabian Sea. *Marine Geology* 201:35–51.

Clemens, S. C., W. L. Prell, D. Murray, G. Shimmield, and G. Weedon. 1991. Forcing mechanisms of the Indian Ocean monsoon. *Nature* 353:720–725.

CLIMAP Project Members. 1976. The surface of the ice-age earth. *Science* 191:1131–1137.

COHMAP Members. 1988. Climatic changes of the last 18,000 years: observations and model simulations. *Science* 241:1043–1052.

Conroy, J. L., and J. T. Overpeck. 2011. Regionalization of present-day precipitation in the greater monsoon region of Asia. *Journal of Climate* 24: 4073–4095.

Cremaschi, M. 2002. Late Pleistocene and Holocene climatic changes in the central Sahara: the case study of the south-western Fezzan, Libya. In *Droughts, food and culture: ecological change and food security in Africa's later prehistory*. F. A. Hassan, ed. Pp. 65–81. New York: Kluwer/Plenum.

Dansgaard, W., S. J. Johnsen, H. B. Clausen, D. Dahl-Jensen, N. S. Gundestrup, C. U. Hammer, C. S. Hvidberg, et al. 1993. Evidence for general instability of past climate from a 250 kyr ice core. *Nature* 364:218–219.

De Boer, B., R. S. W. van de Wal, R. Bintanja, L. J. Lourens, and E. Tuenter. 2010. Cenozoic global ice-volume and temperature simulations with 1-D ice-sheet models forced by benthic $\delta^{18}O$ records. *Annals of Glaciology* 51: 23–33.

De Boer, B., R. S. W. van de Wal, L. J. Lourens, and R. Bintanja. 2011. Transient nature of the earth's climate and the implications for the interpretation of benthic records. *Palaeogeography, Palaeoclimatology, Palaeoecology* 335/336: 4–11.

deMenocal, P., J. Bloemendal, and J. King. 1991. A rock-magnetic record of monsoonal dust deposition to the Arabian Sea: evidence for a shift in the mode of deposition at 2.4 Ma. In *Proceedings of the Ocean Drilling Program, Scientific Results*, vol. 117. Pp. 389–407. College Station, TX: Ocean Drilling Program.

Derricourt, R. 2005. Getting "out of Africa": sea crossings, land crossings and culture in the hominin migrations. *Journal of World Prehistory* 19:119–132.

Drake, N. A., R. M. Blench, S. J. Armitage, C. S. Bristow, and K. H. White. 2011. Ancient watercourses and biogeography of the Sahara explain the peopling of the desert. *Proceedings of the National Academy of Sciences of the USA* 108:458–462.

Duce, R. A., P. S. Liss, J. T. Merrill, E. L. Atlas, P. Buat-Menard, B. B. Hicks, J. M. Miller, et al. 1991. The atmospheric input of trace species to the world ocean. *Global Biogeochemical Cycles* 5:193–259.

El-Fandy, M. G. 1946. Barometric lows of Cyprus. *Quarterly Journal of the Royal Meteorological Society* 72:291–306.

Emeis, K. C., T. Sakamoto, R. Wehausen, and H. J. Brumsack. 2000. The sapropel record of the eastern Mediterranean Sea: results of Ocean Drilling Program Leg 160. *Palaeogeography, Palaeoclimatology, Palaeoecology* 158: 371–395.

EPICA (European Project for Ice Coring in Antarctica) Community Members. 2006. One-to-one coupling of glacial climate variability in Greenland and Antarctica. *Nature* 444:195–197.

Fenton, M., S. Geiselhart, E. J. Rohling, and C. Hemleben. 2000. Aplanktonic zones in the Red Sea. *Marine Micropaleontology* 40:277–294.

Fernandes, C., E. J. Rohling, and M. Siddall. 2006. Absence of Quaternary Red Sea land bridges: biogeographic implications. *Journal of Biogeography* 33:961–966.

Fernandes, V., F. Alshamali, M. Alves, M. D. Costa, J. B. Pereira, N. M. Silva, L. Cherni, et al. 2012. The Arabian cradle: mitochondrial relicts of the first steps along the southern route out of Africa. *American Journal of Human Genetics* 90:1–9.

Fleitmann, D., S. J. Burns, A. Mangini, M. Mudelsee, J. Kramers, I. Villa, U. Neff, et al. 2007. Holocene ITCZ and Indian monsoon dynamics recorded in stalagmites from Oman and Yemen (Socotra). *Quaternary Science Reviews* 26:170–188.

Fleitmann, D., S. J. Burns, M. Mudelsee, U. Neff, J. Kramers, A. Mangini, and A. Matter. 2003*a*. Holocene forcing of the Indian monsoon recorded in a stalagmite from Southern Oman. *Science* 300:1737–1739.

Fleitmann, D., S. J. Burns, U. Neff, A. Mangini, and A. Matter. 2003*b*. Changing moisture sources over the last 330,000 years in Northern Oman from fluid-inclusion evidence in speleothems. *Quaternary Research* 60:223–232.

Fleitmann, D., S. J. Burns, U. Neff, M. Mudelsee, A. Mangini, and A. Matter. 2004. Palaeoclimatic interpretation of high-resolution oxygen isotope profiles derived from annually laminated speleothems from Southern Oman. *Quaternary Science Reviews* 23:935–945.

Foley, J. A., M. T. Coe, M. Scheffer, and G. Wang. 2003. Regime shifts in the Sahara and Sahel: interactions between ecological and climatic systems in Northern Africa. *Ecosystems* 6:524–539.

Frigola, J., A. Moreno, I. Cacho, M. Canals, F. J. Sierro, J. A. Flores, J. O. Grimalt, D. A. Hodell, and J. H. Curtis. 2007. Holocene climate variability in the western Mediterranean region from a deepwater sediment record. *Paleoceanography* 22:PA2209, doi:10.1029/2006PA001307.

Gasse, F. 2000. Hydrological changes in the African tropics since the Last Glacial Maximum. *Quaternary Science Reviews* 19:189–211.

Gaven, C., C. Hillaire-Marcel, and N. Petit-Maire. 1981. A Pleistocene lacustrine episode in southeastern Libya. *Nature* 290:131–133.

Ghoneim, E. 2008. Optimum groundwater locations in the northern United Arab Emirates. *International Journal of Remote Sensing* 29:5879–5906.

Goodfriend, G. A. 1991. Holocene trends in ^{18}O in land snail shells from the Negev Desert and their implications for changes in rainfall source areas. *Quaternary Research* 35:417–426.

Grant, K. M., E. J. Rohling, M. Bar-Matthews, A. Ayalon, M. Medina-Elizalde, C. Bronk Ramsey, C. Satow, and A. P. Roberts. 2012. Rapid coupling between ice volume and polar temperature over the past 150 kyr. *Nature* 491: 744–747.

Grootes, P. M., M. Stuiver, J. W. C. White, S. Johnsen, and J. Jouzel. 1993. Comparison of oxygen isotope records from the GISP2 and GRIP Greenland ice cores. *Nature* 366:552–554.

Grün, R., C. Stringer, F. McDermott, R. Nathan, N. Porat, S. Robertson, L. Taylor, G. Mortimer, S. Eggins, and M. McCulloch. 2005. U-series and ESR analyses of bones and teeth relating to the human burials from Skhul. *Journal of Human Evolution* 49:316–334.

Hayes, A., M. Kucera, N. Kallel, L. Sbaffi, and E. J. Rohling. 2005. Glacial Mediterranean sea surface temperatures reconstructed from planktonic foraminiferal assemblages. *Quaternary Science Reviews* 24:999–1016.

Hays, J. D., J. Imbrie, and N. J. Shackleton. 1976. Variations in the earth's orbit: pacemaker of the ice ages. *Science* 194:1121–1132.

Hemming, S. R. 2004. Heinrich events: massive Late Pleistocene detritus layers of the North Atlantic and their global imprint. *Reviews of Geophysics* 42:1–43.

Hickey, B., and A. S. Goudie. 2007. The use of TOMS and MODIS to identify dust storm source areas: the Tokar delta (Sudan) and the Seistan basin (south west Asia). In *Geomorphological variations*. A. S. Goudie, and J. Kalvoda, J., eds. Pp. 37–57. Prague: P3K.

Hilgen, F. J. 1991. Astronomical calibration of Gauss to Matuyama sapropels in the Mediterranean and implication for the geomagnetic polarity time scale. *Earth and Planetary Science Letters* 104:226−244.

Hilgen, F. J., L. J. Lourens, A. Berger, and M. F. Loutre. 1993. Evaluation of the astronomically calibrated time-scale for the late Pliocene and earliest Pleistocene. *Paleoceanography* 8:549−565.

Imbrie, J., and J. Z. Imbrie. 1980. Modeling the climatic response to orbital variations. *Science* 207:943–953.

Imbrie, J., and K. P Imbrie. 1986. *Ice ages: solving the mystery*. Cambridge, MA: Harvard University Press.

Ivanochko, T. S., R. S. Ganeshram, G. J. A. Brummer, G. Ganssen, S. J. A.

Jung, S. G. Moreton, and D. Kroon. 2005. Variations in tropical convection as an amplifier of global climate change at the millennial scale. *Earth and Planetary Science Letters* 235:302–314.

Jiang, H., J. T. Farrar, R. C. Beardsley, R. Chen, and C. Chen. 2009. Zonal surface wind jets across the Red Sea due to mountain gap forcing along both sides of the Red Sea. *Geophysical Research Letters* 36:L19605, doi: 10.1029/2009GL040008.

Jouzel, J., V. Masson-Delmotte, O. Cattani, G. Dreyfus, S. Falourd, G. Hoffmann, B. Minster, et al. 2007. Orbital and millennial Antarctic climate variability over the past 800,000 years. *Science* 317:793–797.

Klein, A. G., B. Isacks, and A. L. Bloom. 1995. Modern and Last Glacial Maximum snowline in Peru and Bolivia: implications for regional climatic change. *Bulletin de l'Institut Français d'Etudes Andines* 24:607–617.

Kopp, R. E., F. J. Simons, J. X. Mitrovica, A. C. Maloof, and M. Oppenheimer. 2009. Probabilistic assessment of sea level during the last interglacial stage. *Nature* 462:863–868.

Kottek, M., J. Grieser, C. Beck, B. Rudolf, and F. Rubel. 2006. World map of the Köppen-Geiger climate classification updated. *Meteorologische Zeitschrift* 15:259–263.

Kotthoff, U., U. C. Muller, J. Pross, G. Schmiedl, I. T. Lawson, and H. Schulz. 2008. Late glacial and Holocene vegetation dynamics in the Aegean region: an integrated view based on pollen data from marine and terrestrial archives. *Holocene* 18:1019–1032.

Kroon, D., I. Alexander, M. Little, L. J. Lourens, A. Matthewson, A. H. F. Robertson, and T. Sakamoto. 1998. Oxygen isotope and sapropel stratigraphy in the Eastern Mediterranean during the last 3.2 million years. In *Proceedings of the Ocean Drilling Program, Scientific Results*, vol. 160. Pp. 181–190. College Station, TX: Ocean Drilling Program.

Kuhlemann, J., E. J. Rohling, I. Kumrei, P. Kubik, S. Ivy-Ochs, and M. Kucera. 2008. Regional synthesis of Mediterranean atmospheric circulation during the Last Glacial Maximum. *Science* 321:1338–1340.

Kuper, R., and S. Kröpelin. 2006. Climate-controlled Holocene occupation in the Sahara: motor of Africa's evolution. *Science* 313:803–807.

Kutzbach, J. E., and R. G. Gallimore. 1988. Sensitivity of a coupled atmosphere/mixed layer ocean model to changes in orbital forcing at 9000 years. *Journal of Geophysical Research* 93:803–821.

Kutzbach, J. E., and P. J. Guetter. 1986. The influence of changing orbital parameters and surface boundary conditions on climate simulations for the past 18,000 years. *Journal of Atmospheric Science* 43:1726–1759.

Kutzbach, J. E., and F. A. Street-Perrott. 1985. Milankovitch forcing in the level of tropical lakes from 18 to 0 kyr. *Nature* 317:130–134.

Laîné, A., M. Kageyama, P. Braconnot, and R. Alkama. 2009. Impact of greenhouse gas concentration changes on surface energetics in IPSL-CM4: regional warming patterns, land-sea warming ratios, and glacial-interglacial differences. *Journal of Climate* 22:4621–4635.

Lambeck, K., A. Purcell, N. C. Fleming, C. Vita-Finzi, A. M. Alsharekh, and G. M. Bailey. 2011. Sea level and shoreline reconstructions for the Red Sea: isostatic and tectonic considerations and implications for hominin migration out of Africa. *Quaternary Science Reviews* 30:3542–3574.

Lambert, F., B. Delmonte, J. R. Petit, M. Bigler, P. R. Kaufmann, M. A. Hutterli, T. F. Stocker, U. Ruth, J. P. Steffensen, and V. Maggi. 2008. Dust-climate couplings over the past 800,000 years from the EPICA Dome C ice core. *Nature* 452:616–619.

Larrasoaña, J. C., A. P. Roberts, and E. J. Rohling. 2013. Dynamics of green Sahara periods and their role in hominin evolution. *PLoS One* 8:e76514, doi:10.1371/journal.pone.0076514.

Larrasoaña, J. C., A. P. Roberts, E. J. Rohling, M. Winklhofer, and R. Wehausen. 2003. Three million years of monsoon variability over the northern Sahara. *Climate Dynamics* 21:689–698.

Laskar, J., M. Gastineau, F. Joutel, P. Robutel, B. Levrard, et al. 2004. A long-term numerical solution for the insolation quantities of the Earth. *Astronomy and Astrophysics* 428:261–285.

Leaman, K. D., and F. A. Schott. 1991. Hydrographic structure of the convection regime in the Gulf of Lions: winter 1987. *Journal of Physical Oceanography* 21:575–598.

Legge, H. L., J. Mutterlose, and H. W. Arz. 2006. Climatic changes in the northern Red Sea during the last 22,000 years as recorded by calcareous nannofossils. *Paleoceanography* 21:PA1003, doi:10.1029/2005PA001142.

Lisiecki, L. E., and M. E. Raymo. 2005. A Plio-Pleistocene stack of 57 globally distributed benthic $\delta^{18}O$ records. *Paleoceanography* 20:PA1003, doi:10.1029/2004PA001071.

Liu, Q., J. C. Larrasoaña, J. Torrent, A. P. Roberts, E. J. Rohling, Z. Liu, and Z. Jiang. 2012. New constraints on climate forcing and variability in the circum-Mediterranean region from magnetic and geochemical observations of sapropels S1, S5 and S6. *Palaeogeography, Palaeoclimatology, Palaeoecology* 333/334:1–12.

Lolis, C. J., A. Bartzokas, and B. D. Katsoulis. 2002. Spatial and temporal 850 hPa air temperature and sea-surface temperature covariances in the Mediterranean region and their connection to atmospheric circulation. *International Journal of Climatology* 22:663–676.

Lourens, L. J., A. Antonarakou, F. J. Hilgen, A. A. M. van Hoof, C. Vergnaud-Grazzini, and W. J. Zachariasse. 1996. Evaluation of the Plio-Pleistocene astronomical timescale. *Paleoceanography* 11:391–413.

Lourens, L. J., R. Wehausen, and H. J. Brumsack. 2001. Geological constraints on tidal dissipation and dynamical ellipticity of the earth over the past three million years. *Nature* 409:1029–1033.

Maheras, P., E. Xoplaki, T. Davies, J. Martin-Vide, M. Bariendos, and M. J. Alcoforado. 1999. Warm and cold monthly anomalies across the Mediterranean basin and their relationship with circulation 1860–1990. *International Journal of Climatology* 19:1697–1715.

Maillard, C., and G. Soliman. 1986. Hydrography of the Red Sea and exchanges with the Indian Ocean in summer. *Oceanologica Acta* 9:249–269.

Malanotte-Rizzoli, P., and A. Bergamasco. 1991. The wind and thermally driven circulation of the eastern Mediterranean Sea. 2. The baroclinic case. *Dynamics of Atmospheres and Oceans* 15:355–419.

Mandel, R. D., and A. H. Simmons. 2001. Prehistoric occupation of Late Quaternary landscapes near Kharga Oasis, western desert of Egypt. *Geoarchaeology* 16:95–117.

MARGO Project Members. 2009. Constraints on the magnitude and patterns of ocean cooling at the Last Glacial Maximum. *Nature Geoscience* 2:127–132.

Martrat, B., J. O. Grimalt, C. Lopez-Martinez, I. Cacho, F. J. Sierro, J. A. Flores, R. Zahn, M. Canals, J. H. Curtis, and D. A. Hodell. 2004. Abrupt temperature changes in the western Mediterranean over the past 250,000 years. *Science* 306:1762–1765.

Matthews, A., A. Ayalon, and M. Bar-Matthews. 2000. D/H ratios of fluid inclusions of Soreq Cave (Israel) speleothems as a guide to the Eastern Mediterranean Meteoric Line relationships in the last 120 ky. *Chemical Geology* 166:183–191.

Mayewski, P. A., L. D. Meeker, M. S. Twickler, S. Whitlow, Q. Yang, W. B. Lyons, and M. Prentice. 1997. Major features and forcing of high-latitude Northern Hemisphere atmospheric circulation using a 110,000-year-long glaciochemical series. *Journal of Geophysical Research* 102:26345–26366.

McDougall, I., F. H. Brown, and J. G. Fleagle. 2005. Stratigraphic placement and age of modern humans from Kibish, Ethiopia. *Nature* 433:733–736.

———. 2008. Sapropels and the age of hominins Omo I and II, Kibish, Ethiopia. *Journal of Human Evolution* 55:409–420.

McGarry, S., M. Bar-Matthews, A. Matthews, A. Vaks, B. Schilman, and A. Ayalon. 2004. Constraints on hydrological and paleotemperature variations in the eastern Mediterranean region in the last 140 ka given by the δD values of speleothem fluid inclusions. *Quaternary Science Reviews* 23:919–934.

Mercone, D., J. Thomson, R. H. Abu-Zied, I. W. Croudace, and E. J. Rohling. 2001. High-resolution geochemical and micropalaeontological profiling of the most recent eastern Mediterranean sapropel. *Marine Geology* 177:25–44.

Middleton, N. J., and A. S. Goudie. 2001. Saharan dust: sources and trajectories. *Transactions of the Institute of British Geographers* 26:165–181.

Milankovitch, M. 1941. *Kanon der Erdbestrahlung und seine Anwendung auf das Eiszeitenproblem.* Royal Serbian Academy Special Publications, vol. 132; Section Mathematics and Natural Sciences, vol. 33. Belgrade: Royal Serbian Academy.

Morcos, S. A. 1970. Physical and chemical oceanography of the Red Sea. *Oceanography and Marine Biology* 8:73–202.

Moreno, A., I. Cacho, M. Canals, M. A. Prins, M. F. Sánchez-Goñi, J. O. Grimalt, and G. J. Weltje. 2002. Saharan dust transport and high-latitude glacial climatic variability: the Alboran Sea record. *Quaternary Research* 58:318–328.

Muhs, D., K. R. Simmons, R. R. Schumann, and R. B. Halley. 2011. Sea-level history of the past two interglacial periods: new evidence from U-series dating of reef corals from south Florida. *Quaternary Science Reviews* 30:570–590.

Müller, U., and J. Pross. 2007. Lesson from the past: present insolation minimum holds potential for glacial inception. *Quaternary Science Reviews* 26:3025–3029.

Naval Oceanography Command. 1987. *U.S. Navy climatic study of the Mediterranean Sea.* Ashville, NC: Naval Oceanography Command Detachment.
Nof, D. 1979. On man-induced variations in the circulation of the Mediterranean Sea. *Tellus* 31:558–564.
Osborne, A. H., D. Vance, E. J. Rohling, N. Barton, M. Rogerson, and N. Fello. 2008. A humid corridor across the Sahara for the migration "out of Africa" of early modern humans 120,000 years ago. *Proceedings of the National Academy of Sciences of the USA* 105:16444–16447.
Osmond, J. K., and A. A. Dabous. 2004. Timing and intensity of groundwater movement during Egyptian Sahara pluvial periods by U-series analysis of secondary U in ores and carbonates. *Quaternary Research* 61:85–94.
Pachur, H. J. 2001. Holozäne Klimawechsel in den nördlichen Subtropen. *Nova Acta Leopoldina NF88* 331:109–131.
Pachur, H. J., and N. Altmann. 2006. *Die Ostsahara im Spätquartär.* Berlin: Springer.
Pachur, H. J., and G. Braun. 1980. The paleoclimate of the central Sahara, Libya and the Libyan Desert. *Palaeoecology of Africa* 12:351–363.
Paillou, P., M. Schuster, S. Tooth, T. Farr, A. Rosenqvist, S. Lopez, and J. M. Malezieux. 2009. Mapping of a major paleodrainage system in eastern Libya using orbital imaging radar: the Kufrah River. *Earth and Planetary Science Letters* 277:327–333.
Parker, A. G., and J. I. Rose. 2008. Climate change and human origins in southeastern Arabia. *Proceedings of the Seminar on Arabian Studies* 38:25–42.
Patzert, W. C. 1974. Wind induced reversal in Red Sea circulation. *Deep-Sea Research* 21:109–121.
Pedgley, D. E. 1974. An outline of the weather and climate of the Red Sea. *Publications Centre National pour l'Exploitation des Oceans, Actes du Colloques* 2:9–21.
Petraglia, M. D. 2011. Trailblazers across Arabia. *Nature* 470:50–51.
Porter, S. C., and Z. An. 1995. Correlation between climate events in the North Atlantic and China during the last glaciation. *Nature* 375:305–308.
Poulos, S. E., P. G. Drakopoulos, and M. B. Collins. 1997. Seasonal variability in sea surface oceanographic conditions in the Aegean Sea (eastern Mediterranean): an overview. *Journal of Marine Systems* 13:225–244.
Prell, W. L., and J. E. Kutzbach. 1987. Monsoon variability over the past 150,000 years. *Journal of Geophysical Research* 92:8411–8425.
Privett, D. W. 1959. Monthly charts of evaporation from the North Indian Ocean, including the Red Sea and Persian Gulf. *Quarterly Journal of the Meteorological Society* 85:424–428.
Reichart, G. J. 1997. Late Quaternary variability of the Arabian Sea monsoon and oxygen minimum zone. Geologica Ultraiectina, no. 154. PhD thesis, Universiteit Utrecht.
Reichart, G. J., L. J. Lourens, and W. J. Zachariasse. 1998. Temporal variability in the northern Arabian Sea oxygen minimum zone (OMZ) during the last 225,000 years. *Paleoceanography* 13:607–621.
Roberts, A. P., E. J. Rohling, K. M. Grant, J. C. Larrasoaña, and Q. Liu. 2011. Atmospheric dust variability from major global source regions over the last 500,000 years. *Quaternary Science Reviews* 30:3537–3541.
Rodwell, M. J., and B. J. Hoskins. 1996. Monsoons and the dynamics of deserts. *Quarterly Journal of the Royal Meteorological Society* 122:1385–1404.
Rohling, E. J. 1994. Review and new aspects concerning the formation of Mediterranean sapropels *Marine Geology* 122:1–28.
———. 1999. Environmental controls on salinity and $\delta^{18}O$ in the Mediterranean. *Paleoceanography* 14:706–715.
———. 2013. Quantitative assessment of glacial fluctuations in the level of Lake Lisan, Dead Sea rift. *Quaternary Science Reviews* 70:63–72.
Rohling, E. J., R. Abu-Zied, J. S. L. Casford, A. Hayes, and B. A. A. Hoogakker. 2009*a*. The marine environment: present and past. In *The physical geography of the Mediterranean.* J. C. Woodward, ed. Pp. 33–67. Oxford: Oxford University Press.
Rohling, E. J., K. Braun, K. Grant, M. Kucera, A. P. Roberts, M. Siddall, and G. Trommer. 2010. Comparison between Holocene and marine isotope stage-11 sea-level histories. *Earth and Planetary Science Letters* 291:97–105.
Rohling, E. J., and H. L. Bryden. 1992. Man-induced salinity and temperature increases in Western Mediterranean Deep Water. *Journal of Geophysical Research* 97:11191–11198.
Rohling, E. J., T. R. Cane, S. Cooke, M. Sprovieri, I. Bouloubassi, K. C. Emeis, R. Schiebel, et al. 2002*a*. African monsoon variability during the previous interglacial maximum. *Earth and Planetary Science Letters* 202:61–75.
Rohling, E. J., M. Fenton, F. J. Jorissen, P. Bertrand, G. Ganssen, and J. P. Caulet. 1998*a*. Magnitudes of sea-level lowstands of the past 500,000 years. *Nature* 394:162–165.
Rohling, E. J., K. Grant, M. Bolshaw, A. P. Roberts, M. Siddall, C. Hemleben, and M. Kucera. 2009*b*. Antarctic temperature and global sea level closely coupled over the past five glacial cycles. *Nature Geoscience* 2:500–504.
Rohling, E. J., K. Grant, C. Hemleben, M. Kucera, A. P. Roberts, I. Schmeltzer, H. Schulz, M. Siccha, M. Siddall, and G. Trommer. 2008*a*. New constraints on the timing and amplitude of sea level fluctuations during Marine Isotope Stage 3. *Paleoceanography* 23:PA3219, doi:10.1029/2008PA001617.
Rohling, E. J., K. Grant, C. Hemleben, M. Siddall, B. A. A. Hoogakker, M. Bolshaw, and M. Kucera. 2008*b*. High rates of sea-level rise during the last interglacial period. *Nature Geoscience* 1:38–42.
Rohling, E. J., A. Hayes, D. Kroon, S. De Rijk, and W. J. Zachariasse. 1998*b*. Abrupt cold spells in the NW Mediterranean. *Paleoceanography* 13:316–322.
Rohling, E. J., and F. J. Hilgen. 1991. The eastern Mediterranean climate at times of sapropel formation: a review. *Geologie en Mijnbouw* 70:253–264.
Rohling, E. J., Q. Liu, A. P. Roberts, J. D. Stanford, S. O. Rasmussen, P. L. Langen, and M. Siddall. 2009*c*. Controls on the East Asian monsoon during the last glacial cycle, based on comparison between Hulu Cave and polar ice-core records. *Quaternary Science Reviews* 28:3291–3302.
Rohling, E. J., R. Marsh, N. J. Wells, M. Siddall, and N. Edwards. 2004*a*. Similar melt-water contributions to glacial sea-level variability from antarctic and northern ice sheets. *Nature* 430:1016–1021.
Rohling, E. J., P. A. Mayewski, and P. Challenor. 2003. On the timing and mechanism of millennial-scale climate variability during the last glacial cycle. *Climate Dynamics* 20:257–267.
Rohling, E. J., P. A. Mayewski, A. Hayes, R. H. Abu-Zied, and J. S. L. Casford. 2002*b*. Holocene atmosphere-ocean interactions: records from Greenland and the Aegean Sea. *Climate Dynamics* 18:587–593.
Rohling, E. J., M. Medina-Elizalde, J. G. Shepherd, M. Siddall, and J. D. Stanford. 2012. Sea surface and high-latitude temperature sensitivity to radiative forcing of climate over several glacial cycles. *Journal of Climate* 25:1635–1656.
Rohling, E. J., M. Sprovieri, T. R. Cane, J. S. L. Casford, S. Cooke, I. Bouloubassi, and K. C. Emeis. 2004*b*. Reconstructing past planktic foraminiferal habitats using stable isotope data: a case history for Mediterranean sapropel S5. *Marine Micropaleontology* 50:89–123.
Rossignol-Strick, M. 1985. Mediterranean Quaternary sapropels, an immediate response of the African monsoon to variation of insolation. *Palaeogeography, Palaeoclimatology, Palaeoecology* 49:237–263.
Rostek, F., E. Bard, L. Beaufort, C. Sonzogni, and G. Ganssen. 1997. Sea surface temperature and productivity records for the past 240 kyr in the Arabian Sea. *Deep Sea Research II* 44:1461–1480.
Rumney, G. R. 1968. *Climatology and the world's climates.* New York: Macmillan.
Ruth, U., M. Bigler, R. Röthlisberger, M. L. Siggaard-Andersen, J. Kipfstuhl, K. Goto-Azuma, M. E. Hansson, S. J. Johnsen, H. Lu, and J. P. Steffensen. 2007. Ice core evidence for a very tight link between North Atlantic and East Asian glacial climate. *Geophysical Research Letters* 34:L03706, doi:10.1029/2006GL027876.
Saaroni, H., A. Bitan, P. Alpert, and B. Ziv. 1996. Continental polar outbreaks into the Levant and Eastern Mediterranean. *International Journal of Climatology* 16:1175–1191.
Said, R. 1981. *The geological evolution of the River Nile.* New York: Springer.
Sánchez-Goñi, M. F., I. Cacho, J. L. Turon, J. Guiot, F. J. Sierro, J. P. Peypouquet, J. O. Grimalt, and N. J. Shackleton. 2002. Synchroneity between marine and terrestrial responses to millennial scale climatic variability during the last glacial period in the Mediterranean region. *Climate Dynamics* 19:95–105.
Schmiedl, G., and D. C. Leuschner. 2005. Oxygenation changes in the deep western Arabian Sea during the last 190,000 years: productivity versus deep-water circulation. *Paleoceanography* 20:A2008, doi:10.1029/2004PA001044.
Schneider von Deimling, T., A. Ganopolski, H. Held and S. Rahmstorf. 2006. How cold was the Last Glacial Maximum? *Geophysical Research Letters* 33: L14709, doi:10.1029/2006GL026484.
Schulz, H., U. von Rad, and H. Erlenkeuser. 1998. Correlation between Arabian Sea and Greenland climate oscillations of the past 110,000 years. *Nature* 393:54–57.
Scrivner, A. E., D. Vance, and E. J. Rohling. 2004. New neodymium isotope data quantify Nile involvement in Mediterranean anoxic episodes. *Geology* 32:565–568.
Shea, J. J. 2008. Transitions or turnovers? climatically-forced extinctions of *Homo sapiens* and Neanderthals in the east Mediterranean Levant. *Quaternary Science Reviews* 27:2253–2270.
Siddall, M., E. J. Rohling, A. Almogi-Labin, C. Hemleben, D. Meischner, I.

Schmeltzer, and D. A. Smeed. 2003. Sea-level fluctuations during the last glacial cycle. *Nature* 423:853–858.
Siddall, M., E. J. Rohling, T. Blunier, and R. Spahni. 2010. Patterns of millennial variability over the last 500 ka. *Climate of the Past* 6:295–303.
Siddall, M., E. J. Rohling, W. G. Thompson, and C. Waelbroeck. 2008. Marine isotope stage 3 sea level fluctuations: data synthesis and new outlook. *Reviews of Geophysics* 46:RG4003, doi:10.1029/2007RG000226.
Siddall, M., D. A. Smeed, C. Hemleben, E. J. Rohling, I. Schmeltzer, and W. R. Peltier. 2004. Understanding the Red Sea response to sea level. *Earth and Planetary Science Letters* 225:421–434.
Sirocko, F., M. Sarnthein, H. Erlenkeuser, H. Lange, M. Arnold, and J. C. Duplessy. 1993. Century-scale events in monsoonal climate over the past 24,000 years. *Nature* 364:322–324.
Stocker, T. F., and S. J. Johnsen. 2003. A minimum thermodynamic model for the bipolar seesaw. *Paleoceanography* 18:1087, doi:10.1029/2003PA000920.
Sun, Y., S. C. Clemens, Z. An, and Z. Yu. 2006. Astronomic timescale and palaeoclimatic implication of stacked 3.6-myr monsoon records from the Chinese loess plateau. *Quaternary Science Reviews* 25:33–48.
Szabo, B. J., C. V. Haynes Jr., and T. A. Maxwell. 1995. Ages of Quaternary pluvial episodes determined by uranium-series and radiocarbon dating of lacustrine deposits of eastern Sahara. *Palaeogeography, Palaeoclimatology, Palaeoecology* 113:227–242.
Tiedemann, R., M. Sarnthein, and N. J. Shackleton. 1994. Astronomical timescale for the Pliocene Atlantic $\delta^{18}O$ and dust flux records of Ocean Drilling Program site 659. *Paleoceanography* 9:619–638.
Trauth, M. H., J. C. Larrasoaña, and M. Mudelsee. 2009. Trends, rhythms and events in Plio-Pleistocene African climate. *Quaternary Science Reviews* 28: 399–411.
Trewartha, G. T. 1966. *The earth's problem climates.* London: Methuen.
Trigo, I. F., T. D. Davies, and G. R. Bigg. 1999. Objective climatology in the Mediterranean region. *Journal of Climate* 12:1685–1696.
———. 2000. Decline in Mediterranean rainfall caused by weakening of Mediterranean cyclones. *Geophysical Research Letters* 27:2913–2916.
Trommer, G., M. Siccha, E. J. Rohling, K. Grant, M. T. J. van der Meer, S. Schouten, U. Baranowski, and M. Kucera. 2011. Sensitivity of Red Sea circulation to sea level and insolation forcing during the last interglacial. *Climate of the Past* 7:941–955.
Trommer, G., M. Siccha, E. J. Rohling, K. Grant, M. T. J. van der Meer, S. Schouten, C. Hemleben, and M. Kucera. 2010. Millennial scale variability in Red Sea circulation in response to Holocene insolation forcing. *Paleoceanography* 25:PA3203, doi:10.1029/2009PA001826.
Tzedakis, P. C. 1999. The last climatic cycle at Kopais, central Greece. *Journal of the Geological Society, London* 156:425–434.
———. 2009. Cenozoic climate and vegetation change. In *The physical geography of the Mediterranean.* J. C. Woodward, ed. Pp. 89–137. Oxford: Oxford University Press.
Tzedakis, P. C., M. R. Frogley, I. T. Lawson, R. C. Preece, I. Cacho, and L. de Abreu. 2004. Ecological thresholds and patterns of millennial-scale climate variability: the response of vegetation in Greece during the last glacial period. *Geology* 32:109–112.
Vaks, A., M. Bar-Matthews, A. Ayalon, A. Matthews, L. Halicz, and A. Frumkin. 2007. Desert speleothems reveal climatic window for African exodus of early modern humans. *Geology* 35:831–834.
Waelbroeck, C., L. Labeyrie, E. Michel, J. C. Duplessy, J. F. McManus, K. Lambeck, E. Balbon, and M. Labracherie. 2002. Sea-level and deep water temperature changes derived from benthic foraminifera isotopic records. *Quaternary Science Reviews* 21:295–305.
Wahby, S. D., and N. F. Bishara. 1981. The effect of the river Nile on Mediterranean water, before and after the construction of the High Dam at Aswan. In *River inputs to ocean systems.* J. M. Martin, J. D. Burton, and D. Eisma, eds. Pp. 311–318. Rome: UNEP-UNESCO.
Wang, X., A. S. Auler, R. L. Edwards, H. Cheng, E. Ito, and M. Solheid. 2006. Interhemispheric anti-phasing of rainfall during the last glacial period. *Quaternary Science Reviews* 25:3391–3403.
Wang, X. F., A. S. Auler, R. L. Edwards, H. Cheng, P. S. Cristalli, P. L. Smart, D. A. Richards, and C. C. Shen. 2004. Wet periods in northeastern Brazil over the past 210 ka linked to distant climate anomalies. *Nature* 432:740–743.
Wehausen, R., and H. J. Brumsack. 2000. Chemical cycles in Pliocene sapropel-bearing and sapropel-barren eastern Mediterranean sediments. *Palaeogeography, Palaeoclimatology, Palaeoecology* 158:325–352.
Whiteman, A. 1971. *The geology of the Sudan Republic.* Oxford: Clarendon.
Williams, M. A. J., D. A. Adamson, B. Cock, and R. McEvedy. 2000. Late Quaternary environments in the White Nile region, Sudan. *Global and Planetary Change* 26:305–316.
Winckler, G., R. F. Anderson, M. Q. Fleisher, D. McGee, and N. Mahowald. 2008. Covariant glacial-interglacial dust fluxes in the equatorial Pacific and Antarctica. *Science* 320:93–96.
Wolff, E. W., J. Chappellaz, T. Blunier, S. O. Rasmussen, and A. Svensson. 2010. Millennial-scale variability during the last glacial: the ice core record. *Quaternary Science Reviews* 29:2828–2838.
Yuan, D., H. Cheng, R. L. Edwards, C. A. Dykoski, M. J. Kelly, M. Zhang, J. Qing, et al. 2004. Timing, duration, and transitions of the last interglacial Asian monsoon. *Science* 304:575–578.

Figure Captions

Figure 1. Summary map of the main climate zones in the study region using the Köppen-Geiger climate classification. C is warm temperate; B is arid; A is equatorial; D is snow; s is summer dry; f is fully humid; S is steppe; W is desert; w is winter dry; m is monsoonal; a is hot summer; b is warm summer; k is cold arid; and h is hot arid. Modified after Kottek et al. (2006).

Figure 2. Atmospheric circulation pattern during Northern Hemisphere summer. The main winds are indicated as arrows. ITCZ = Inter-Tropical Convergence Zone; H = areas of high sea-level pressure; L = areas of low sea-level pressure. After an adaptation in Rohling et al. (2009), which compiled information from Rossignol- Strick (1985) and Reichart (1997).

Figure 3. Topography of the Red Sea basin. The dashed line delineates the Red Sea watershed. Numbers refer to key sediment core locations (not used here). After Siddall et al. (2004).

Figure 4. Comparison between three approaches for reconstructing continuous records of sea-level variations. Black is Waelbroeck et al. (2002) based on coral-calibrated deep-sea stable oxygen isotope data, with uncertainties (grey). Green dashed line is the reconstruction of De Boer et al. (2010, 2011) from a model-based deconvolution of deep-sea stable oxygen isotope records into a temperature and a sea-level component, following the method of Bintanja et al. (2005). Red dots with orange (2σ) uncertainty bars represent the Red Sea reconstruction on a U-Th adjusted chronology (Rohling et al., 2009b, 2010). Modified after Rohling et al. (2012).

Figure 5. Major global dust sources and locations of dust records. Dust flux contours (mg m^{-2} yr^{-1}) are shown in oceans surrounding dust sources (after Duce et al., 1991). Locations of dust records discussed are indicated (Ocean Drilling Program sites 659 (Tiedemann et al., 1994), 721 (deMenocal et al., 1991), and 967 (Larrasoaña et al., 2003), and the Zhaojiachuan and Lingtai loess sections (Sun et al., 2006)). Site KL09 is the Red Sea record presented in Rohling et al. (2008b, 2009b) and Roberts et al. (2011). Modified after Roberts et al. (2011).

Figure 6. Comparison of sea level and dust records for the Red Sea, circum-Sahara region, and Chinese Loess Plateau. (a) Central Red Sea sea-level reconstruction (Rohling et al., 2009b, 2010). (b) Environmental magnetic IRM900 mT@AF120 mT proxy for windblown hematite (Hem.) in Red Sea core KL09 (grey) compared to the stacked Chinese loess grainsize record from Zhaojiachuan and Lingtai, Chinese Loess Plateau (red; from Sun et al., 2006, with minor age adjustments in Roberts et al., 2011). Panels (c), (d), (e), and (f), respectively, compare the Red Sea dust record (grey shading) with dust records from EPICA Dome C, Antarctica (Lambert et al., 2008), ODP Site 659, off northwest Africa (Tiedemann et al., 1994), ODP Site 967, Eastern Mediterranean Sea (Larrasoaña et al., 2003), and ODP Site 721, Arabian Sea (deMenocal et al., 1991). Vertical dashed lines coincide with Red Sea dust peaks at the glacial terminations and are shown to assist comparisons between panels. The Red Sea records are shown for consistency on same (Rohling et al., 2009b, 2010) chronology as used in Roberts et al. (2011). This chronology is (subtly) updated

within the last 150,000 years in Figures 7 and 8, based on the latest age controls developed by Grant et al. (2012).

Figure 7. Comparison of different records of climate variability including polar ice core records, sea level, and Mediterranean temperature variability. (a) The EPICA Dome C ice-core stable hydrogen isotope proxy for temperature, Antarctica (Jouzel et al., 2007); (b) the Red Sea sea-level record in the pre-150 ka interval on the chronology of Rohling et al. (2009b, 2010) and in the post-150 ka interval on the latest chronology using the age constraints developed by Grant et al. (2012); (c) sea surface temperature in the Alboran Sea, westernmost Mediterranean (Martrat et al., 2004); and (d) in grey the stacked North-GRIP ice-core oxygen isotope proxy for temperature, Greenland (Wolff et al., 2010), and – for clarity – in black a 21-point moving average smoothing. Blue bars at the bottom indicate intervals of particularly pronounced millennial-scale climate variability, after the analysis of Siddall et al. (2010).

Figure 8. Direct comparison between: (a) the latest version of the Red Sea sea-level reconstruction, with the pre-150 ka interval on the chronology of Rohling et al. (2009b, 2010) and the post-150 ka interval on the new chronology of Grant et al. (2012); and (b) central Red Sea dust proxy data, including the Ti/Ca ratio from core-scanning XRF analysis (grey), and hematite concentration data from environmental magnetic analyses (red) (see also Rohling et al., 2008b; Roberts et al., 2011). Data originate from a single sampling of the same sedimentary sequence, which ensures unambiguous phase relationships between the various records. Yellow bars are explained in the text. Blue bars indicate intervals of particularly pronounced millennial-scale climate variability, after the analysis of Siddall et al. (2010) (see also Figure 7).

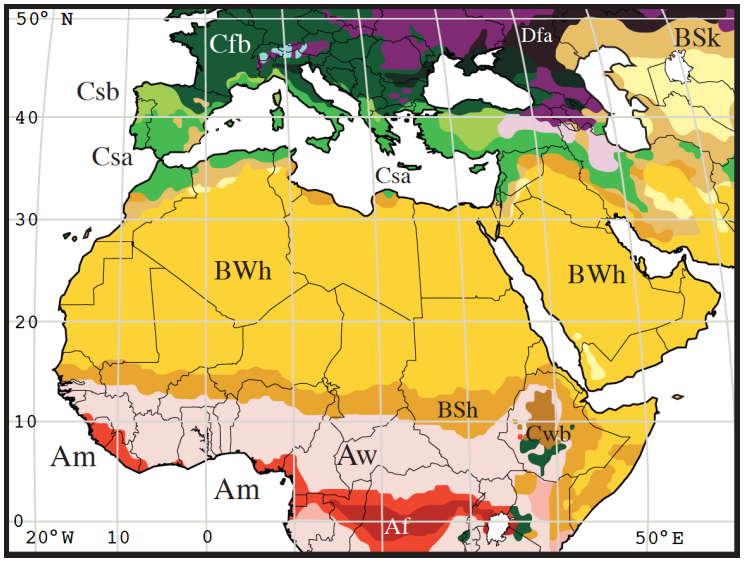

Figure 1.

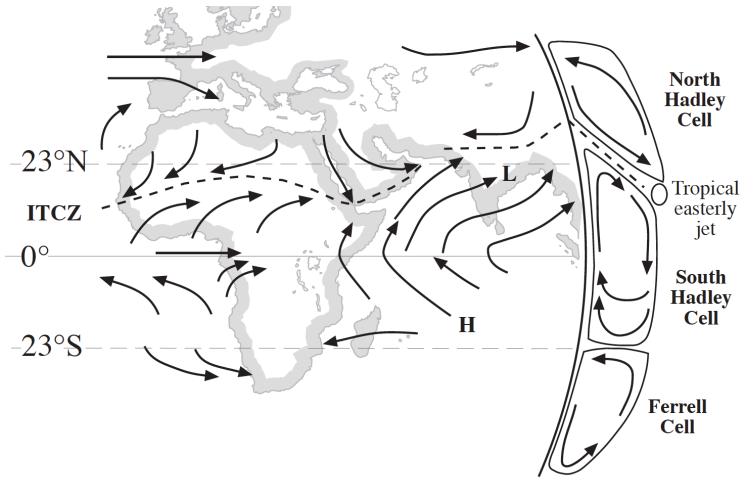

Figure 2.

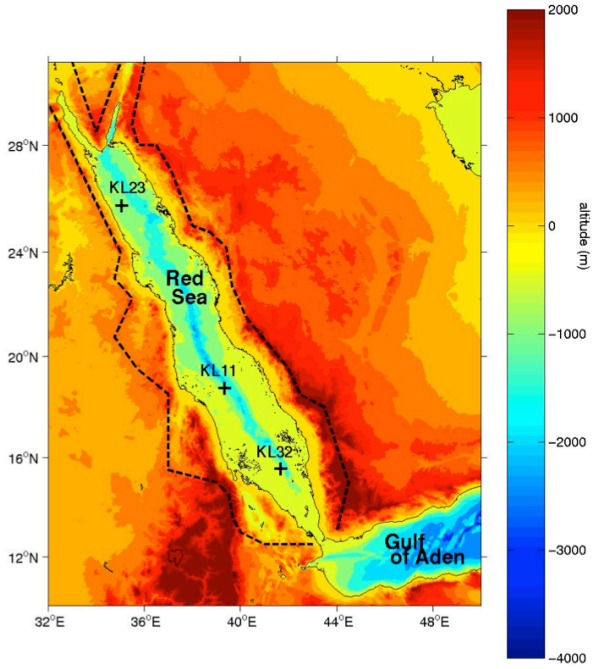

Figure 3.

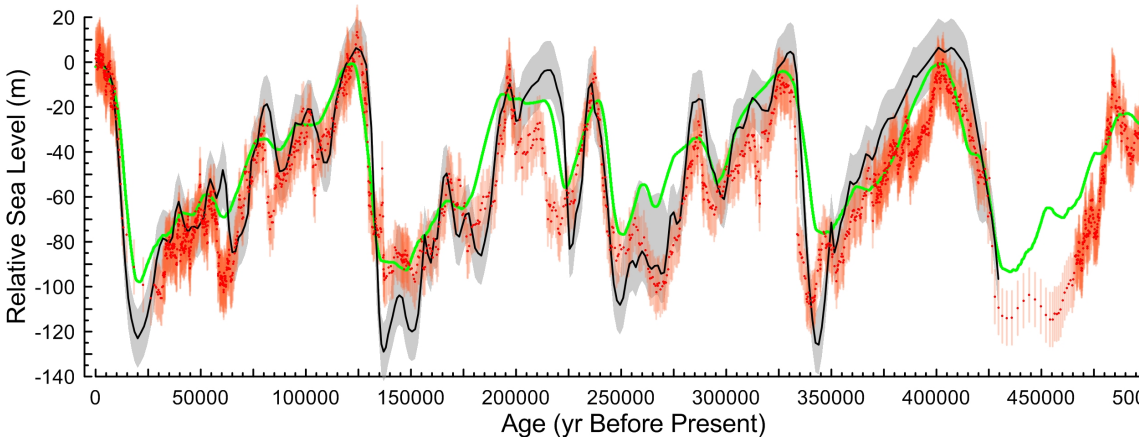

Figure 4.

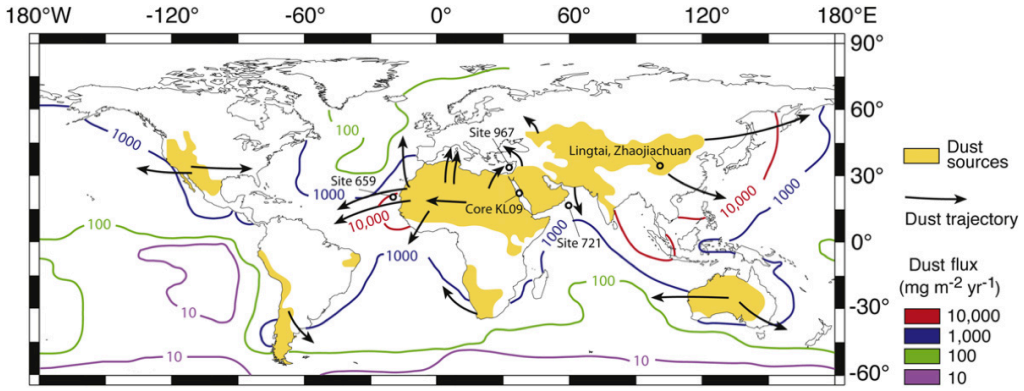

Figure 5.

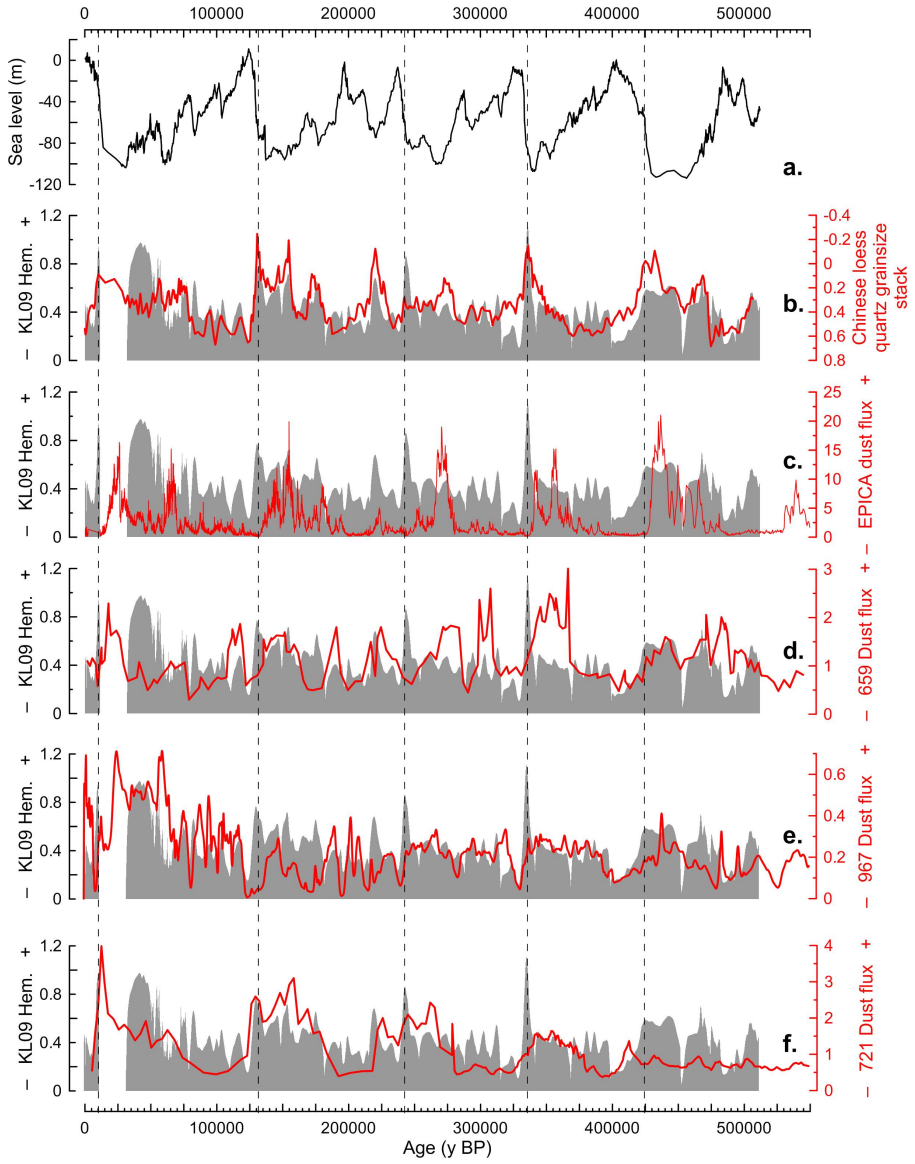
0
100000
200000
300000
400000
500000
Sea level (m)
0
-40
-80
-120
a.
KL09 Hem.
1.2
0.8
0.4
0
b.
Chinese loess quartz grainsize stack
-0.4
-0.2
0
0.2
0.4
0.6
0.8
c.
EPICA dust flux
25
20
15
10
5
0
d.
659 Dust flux
3
2
1
0
e.
967 Dust flux
0.6
0.4
0.2
0
f.
721 Dust flux
4
3
2
1
0
Age (y BP)

Figure 6.

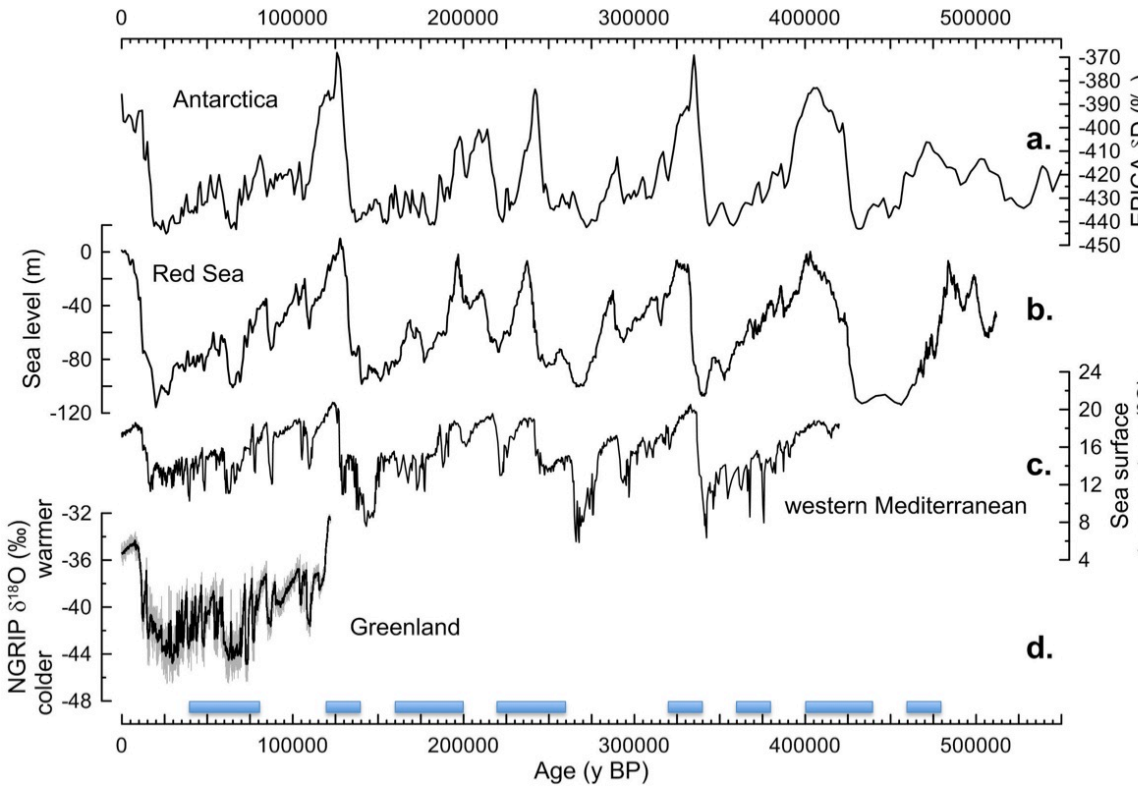

Figure 7.

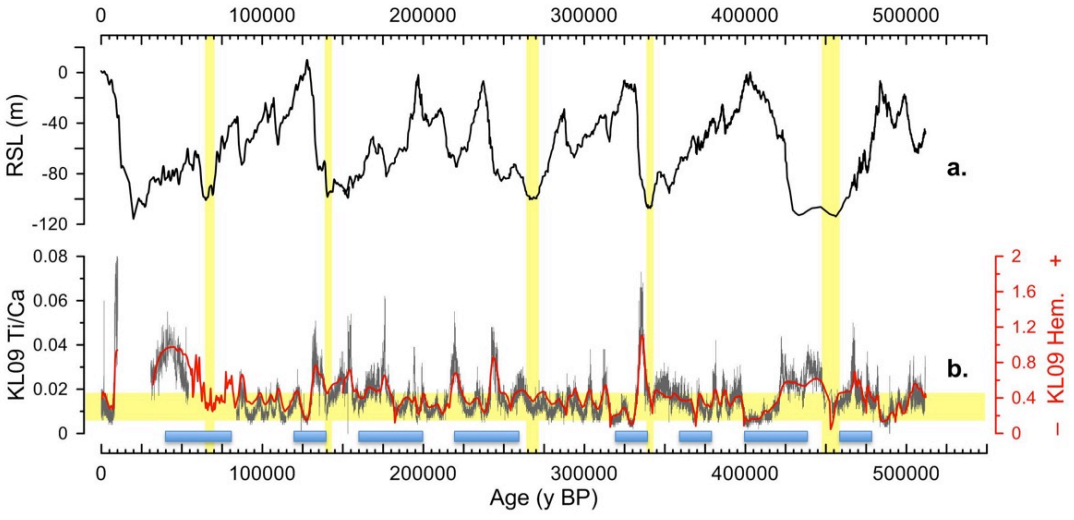

Figure 8.